JEM Journal of Experimental Medicine

ARTICLE

Sensing of apoptotic cells through Axl causes lung basal cell proliferation in inflammatory diseases

Naoya Fujino[1,3*], Oliver J. Brand[1,2*], David J. Morgan[1,2*], Toshifumi Fujimori[1], Aleksander M. Grabiec[1,4], Christopher P. Jagger[1,2], Rose A. Maciewicz[5,6], Mitsuhiro Yamada[3], Koji Itakura[3], Hisatoshi Sugiura[3], Masakazu Ichinose[3], and Tracy Hussell[1,2]

Epithelial cell proliferation, division, and differentiation are critical for barrier repair following inflammation, but the initial trigger for this process is unknown. Here we define that sensing of apoptotic cells by the TAM receptor tyrosine kinase Axl is a critical indicator for tracheal basal cell expansion, cell cycle reentry, and symmetrical cell division. Furthermore, once the pool of tracheal basal cells has expanded, silencing of Axl is required for their differentiation. Genetic depletion of Axl triggers asymmetrical cell division, leading to epithelial differentiation and ciliated cell regeneration. This discovery has implications for conditions associated with epithelial barrier dysfunction, basal cell hyperplasia, and continued turnover of dying cells in patients with chronic inflammatory pulmonary diseases.

Introduction

Basal cells reside at variable frequency throughout the airway epithelium, immediately above the basement membrane, and are responsible for normal epithelial barrier maintenance through transdifferentiation and replenishment (Evans et al., 2001; Hajj et al., 2007; Rock et al., 2009, 2010). The epithelial barrier contains a variety of cell types including ciliated, secretory, and undifferentiated cells (Knight and Holgate, 2003). Replenishment of the appropriate cell type requires intimate contact with adjacent cells and sensing mechanisms to replace the correct damaged compartment (Evans et al., 2001). Basal cells express keratin 5 (Krt5) and -17, integrins ITG-A6, -B1, and -B4, and transcription factors tumor protein p63 (TP63) and basonuclin and are enriched for genes associated with vascular endothelial growth factor, transforming growth factor-β, NF-κB, mitogen-activated protein kinases, and Notch signaling (Hackett et al., 2011; Ryan et al., 2014). This mosaic of potential interactions, together with factors secreted by a damaged epithelial compartment, most likely determines basal cell function and differentiation (Paul et al., 2014; Tadokoro et al., 2014, 2016; Gao et al., 2015; Pardo-Saganta et al., 2015; Balasooriya et al., 2016). Basal cell hyperplasia and a loss of apical ciliated and nonmucous secretory cells are common features of chronic obstructive pulmonary disease (COPD) and suggest that communication to repair the epithelial barrier has gone wrong (Puchelle et al., 2006; Crystal, 2014; Shaykhiev and Crystal, 2014b). In vitro experiments using air–liquid interface cultures suggest that in COPD, excessive secretion of ligands for epidermal growth factor receptors by differentiated airway epithelial cells leads to an abnormal transition of basal cells to squamous epithelial cells and reduced ciliated and SCGB1A1-producing nonmucous secretory cells (Shaykhiev et al., 2013). Therefore, sensing of an abnormal environment can itself lead to progressive disorder of the barrier epithelium.

Basal cells in the adult trachea are dormant in health but reenter the cell cycle to repopulate damaged cells in response to insults such as sulfur dioxide (Borthwick et al., 2001; Rawlins et al., 2009; Tata et al., 2013), naphthalene (Hsu et al., 2014), polidocanol (Paul et al., 2014), and H1N1/PR8 influenza A virus (Buchweitz et al., 2007; Tata et al., 2013). However, the trigger for cell cycle reentry and the decision for proliferation versus differentiation are unclear. We reasoned that another significant component of a damaged environment is the presence of apoptotic cells and that these might be the initiating factor for basal cell proliferation and their hyperplasia in lung disease. Recognition of apoptotic cells by phagocytes restricts inflammatory responses to prevent inflammation and autoimmunity to self (Hochreiter-Hufford and Ravichandran, 2013; Poon et al., 2014;

[1]Manchester Collaborative Centre for Inflammation Research, the University of Manchester, Manchester, UK; [2]Lydia Becker Institute of Immunology and Inflammation, the University of Manchester, Manchester, UK; [3]Department of Respiratory Medicine, Tohoku University Graduate School of Medicine, Sendai, Japan; [4]Department of Microbiology, Faculty of Biochemistry, Biophysics and Biotechnology, Jagiellonian University, Kraków, Poland; [5]Respiratory, Inflammation, and Autoimmunity Innovative Medicines and Early Development Biotech Unit, AstraZeneca, Gothenburg, Sweden; [6]Institute of Infection, Immunity, and Inflammation, University of Glasgow, Glasgow, UK.

*N. Fujino, O.J. Brand, and D.J. Morgan contributed equally to this paper; Correspondence to Tracy Hussell: tracy.hussell@manchester.ac.uk; Naoya Fujino: nfujino@med.tohoku.ac.jp.

Arandjelovic and Ravichandran, 2015). In addition to phagocytes, recognition of apoptotic cells is important for maintaining tissue homeostasis by nonimmune cells, including (i) myoblast fusion in murine skeletal muscles (Hochreiter-Hufford et al., 2013), (ii) lipid metabolism of macrophages in mice (Fond et al., 2015), and (iii) cellular proliferation in *Hydra* (Chera et al., 2009), *Drosophila* (Fan and Bergmann, 2008), and mice (Li et al., 2010). Among these novel roles of apoptotic cells in multiple biological processes, the induction of cellular proliferation (so-called apoptosis-induced compensatory proliferation) is of particular interest due to its relevance to clinical oncology and regenerative medicine (Bergmann and Steller, 2010; Ryoo and Bergmann, 2012). Mitogens, such as Hedgehog or Wnt, released from apoptotic cells in a caspase-dependent manner are postulated to stimulate proliferation of surrounding viable cells.

The TAM (Tyro3, Mer, and Axl) receptor tyrosine kinase family recognizes apoptotic cells by binding the C-terminal sex hormone–binding globulin-like domain of Protein S or Gas6, whose N-terminal Gla domains bridge the TAM receptors to phosphatidylserine on the surface of apoptotic cells (Lemke and Rothlin, 2008; Lemke, 2013). The requirement for different TAM receptor family members is beginning to be unraveled: Mer acts as a tolerogenic receptor under homeostatic conditions, whereas Axl is critical for resolution of inflammation under pathological conditions (Zagórska et al., 2014), including following influenza A virus infection (Fujimori et al., 2015). In oncology, Axl is a potent driver of proliferation, invasion, and metastasis of cancers through epithelial-to-mesenchymal transition (Zhang et al., 2012; Asiedu et al., 2014; Cichoń et al., 2014). In addition, our recent study indicated that Axl regulates differentiation of human lung tissue–derived progenitor cells (Fujino et al., 2017). Axl may therefore recognize cell death during tissue damage and convert this into multiple intracellular signals for cellular proliferation and differentiation.

Beyond apoptotic cell recognition and efferocytosis, the function of TAM receptors, in particular Axl, is not currently known. Here we show that basal cells in tracheal epithelium express Axl that is constitutively bound to the bridging molecule Gas6. Furthermore, in the presence of apoptotic cells, usually dormant basal cells reenter the cell cycle and undergo symmetrical cell division, producing more basal cells. In the absence of Axl, basal cells undergo asymmetric cell division to other epithelial cell components. This is the first time the presence and absence of a single apoptotic cell recognition receptor has been shown to define an alternate cellular outcome. With increased apoptotic cell turnover in the lungs of patients with chronic disease (Hodge et al., 2005), our results also explain the characteristic basal cell hyperplasia and lack of effective barrier repair in these patients. This pathway is targetable and currently of interest in oncology, potentially providing a realistic strategy for a therapeutic regimen targeting this facet of disease.

Results

The TAM receptor Axl is constitutively expressed on tracheal basal cells in the steady state

We first examined whether TAM receptors were expressed on cells in the murine tracheal epithelium. Basal cells, ciliated cells, and two types of secretory cells (SSEA-1–positive or SSEA-1–negative) were purified by FACS, and their identity was confirmed by analyzing lineage-specific markers by quantitative RT-PCR (qRT-PCR; Fig. S1). Only basal cells expressed appreciable levels of Axl compared with other tracheal epithelial cell subsets (Fig. 1 A). Expression was confirmed by immunofluorescence using an anti-mouse Axl antibody that clearly highlighted Axl expression on cells positive for the basal cell markers Krt5 or TP63 (Fig. 1 B). The specificity of this antibody was confirmed before using *Axl*$^{-/-}$ mice (Zagórska et al., 2014) and repeated here (Fig. S1). Interestingly, the other TAM receptors, Mer and Tyro3, were not expressed in any murine tracheal epithelial cell subset, although we could confirm Mer expression on airway macrophages (Fujimori et al., 2015) and Tyro3 on testicular sertoli cells (Lu et al., 1999; Fig. S1). Of total tracheal Axl-expressing cells, 97.7 ± 1.0% or 97.3 ± 1.9% were positive for Krt5 or TP63 (mean ± SEM of five individual mice), respectively, supporting the mRNA data of selective expression of Axl in basal cells. A recent study using single-cell qRT-PCR and lineage labeling identified two distinct subsets of Krt5-expressing basal cells in the murine trachea: a basal stem cell population and a basal luminal progenitor population (Watson et al., 2015). It would appear that Axl is expressed by both, since 94.2 ± 1.4% of total Krt5-expressing basal cells and 95.6 ± 1.4% of total TP63-expressing basal cells express Axl (mean ± SEM of five individual mice). Compared with the lung, there are very few immune cells in the trachea (Fig. S2). We confirmed Axl expression on airway macrophages as reported previously (Fujimori et al., 2015). However, we did not observe any staining on the few immune cell subsets in the trachea, although we cannot rule out expression by very low-frequency cells not detected by flow cytometry.

Gas6 is a specific ligand for Axl and bridges its interaction with externalized phosphatidylserine on apoptotic cells (Lew et al., 2014; Zagórska et al., 2014). Similar to our previous observations of Axl expression on airway macrophages (Fujimori et al., 2015), we observed constitutively bound GAS6 on Krt5-expressing basal cells in WT C57BL/6 mice, but not in Axl knockout mice (Fig. 1 C). Despite the loss of GAS6 from the tracheal epithelium in *Axl*$^{-/-}$, soluble levels similar to WT mice were observed in the plasma (40,000 pg/ml) and airway lavage fluid (4,000 pg/ml), suggesting that GAS6 production was unaffected. Collectively, these data indicate that Axl, but not MerTK or Tyro3, is preferentially expressed on tracheal basal cells and, at homeostasis, constitutively bound to Gas6.

Before analysis of the role of basal cell Axl expression in inflammation, we first examined whether its absence in Axl knockout mice caused cell cycle reentry of this dormant cell population in the steady state. Ki67 is present during all active phases of the cell cycle (G1, S, G2, and mitosis) but is absent from resting cells at G0 (Gerdes et al., 1984). Immunofluorescence staining for Ki67^{+} basal cells (Krt5^{+}) in both WT and *Axl*$^{-/-}$ mice was infrequent (Fig. 1 D), nor was there any difference in total basal cell number (Fig. 1 E) or the number (Fig. 1 F) and proportion (Fig. 1 G) of basal cells in cell cycle in the steady state. Therefore, Axl alone does not cause basal cell proliferation.

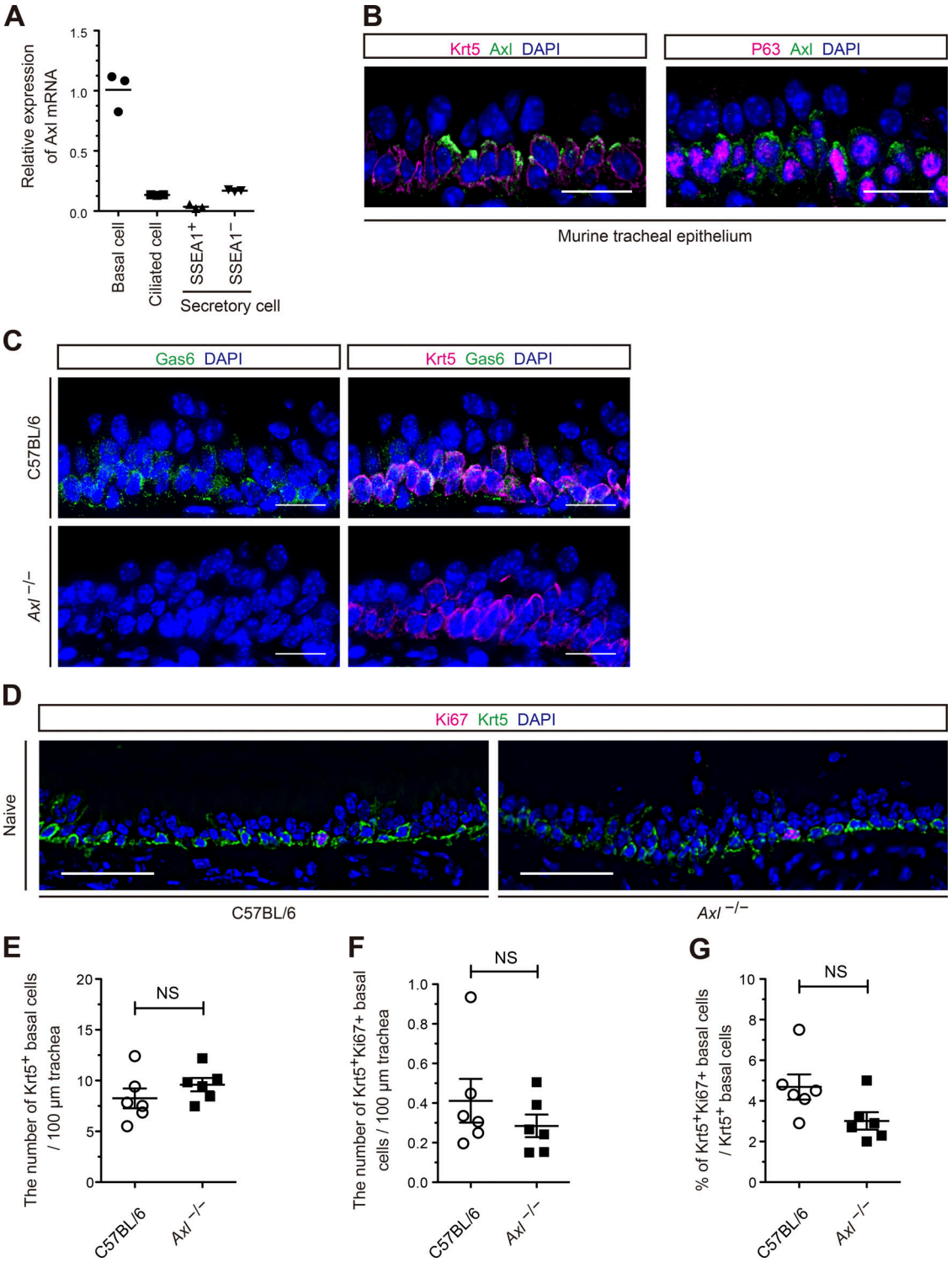

Figure 1. **Axl expression on basal cells in murine tracheal epithelium under homeostatic conditions. (A)** qRT-PCR analysis of *Axl* mRNA expression in epithelial cell subsets sorted from murine trachea. Each symbol represents data pooled from 10 tracheas, and lines indicate the mean value. **(B)** Immunostaining of murine tracheal epithelium indicating apicolateral expression of Axl protein on airway basal cells marked by Krt5 (left panel) or TP63 (right panel) at steady state. **(C)** Immunostaining indicating constitutive binding of Gas6 to Axl expressed on Krt5$^+$ airway basal cells at steady state in WT C57BL/6 or *Axl*$^{-/-}$ mice. **(D)** Immunostaining of murine tracheal epithelium for Ki67$^+$ (magenta)/Krt5$^+$ (green) basal cells in WT C57BL/6 or *Axl*$^{-/-}$ mice. **(E–G)** The number of Krt5$^+$ basal cells per 100 µm trachea (E), the number of Krt5$^+$Ki67$^+$ basal cells per 100 µm trachea (F), and the percentage of Krt5$^+$Ki67$^+$ basal cells to total Krt5$^+$ basal cells (G) between C57BL6 and *Axl*$^{-/-}$ mice at steady state. Data are expressed as mean ± SEM of five individual mice. Scale bars represent 20 µm (B and C) and 50 µm (D).

Axl promotes cell cycle reentry and DNA synthesis of basal cells in influenza-infected mice

Axl is reported to be critical for apoptotic cell recognition during inflammation (Zagórska et al., 2014; Fujimori et al., 2015; Fourgeaud et al., 2016), so a lack of an effect on basal cells in Axl knockout at homeostasis was unsurprising. We therefore next used the H1N1/PR8 influenza A virus infection model as an inflammatory insult for the following reasons. First, the PR8 influenza strain causes a high level of virus replication and severe pulmonary inflammation in C57BL/6 mice compared with other influenza A virus strains including BJx109 and HKx31 (Tate et al., 2011). Second, influenza A virus selectively infects ciliated epithelial cells via α2,3-linked sialic acid, so any damage would be next to basal cells (Ibricevic et al., 2006). Finally, influenza A virus infection induces apoptosis and proliferation of epithelial cells widely in murine tracheas (Buchweitz et al., 2007). We confirmed that intranasal influenza virus infection caused the loss of ciliated epithelial cells (acetylated tubulin–positive) by day 3, with recovery of the epithelial barrier by day 14 (Fig. 2 A).

During influenza virus–induced injury, Axl-expressing basal cells were in close contact with cleaved caspase 3–positive apoptotic epithelial cells (Fig. 2, B and C). Immunofluorescence staining for apoptotic cells within basal cells (cCasp3 and Krt5$^+$ cells) was never observed. Unlike homeostasis (Fig. 1 D), in the context of inflammatory lung disease, basal cells entered the cell cycle, an effect lost in Axl knockout mice (Fig. 2 D). Furthermore, the number of basal cells per 100 µm trachea (Fig. 2 E) and the number and proportion of cycling Ki67$^+$/Krt5$^+$ cells (Fig. 2, F and G) was reduced in Axl knockout mice. A role for Axl in cell cycle reentry was further confirmed in an ex vivo culture, where basal cells sorted from *Axl*$^{-/-}$ mice displayed less Ki67 compared with those sorted from C57BL/6 mice (Fig. S3). In addition, basal cells in the trachea of *Axl*$^{-/-}$ mice sequestered less 5-ethynyl-2′-deoxyuridine (EdU), a thymidine analogue taken up during DNA synthesis, than WT mice (Fig. S3). Taken together, these data show that in an inflammatory setting with apoptotic cells, Axl promotes cell cycle reentry and proliferation of basal cells.

Apoptotic cells are associated with cell cycle reentry of tracheal basal cells via Axl

Despite juxtaposed basal cells and apoptotic cells, inflammation-induced basal cell proliferation could be due to a multitude of other factors. To indicate a direct effect of apoptotic cells, we therefore intranasally delivered murine apoptotic thymocytes into C57BL/6 mice and quantified Ki67-expressing basal cells. The number and percentage of Ki67$^+$/Krt5$^+$ basal cells to total basal cells increased after apoptotic thymocyte administration (Fig. 3, A and B). If apoptotic cells are inducing basal cell proliferation via Axl, then their delivery to Axl knockout mice should have a reduced effect. Total basal cell numbers remained unaffected (not depicted). However, the number and proportion of basal cells entering the cell cycle was significantly reduced in Axl knockout mice (Fig. 3, C–E). These data indicate that apoptotic cells trigger cell cycle reentry and that Axl kinase plays a significant role. The reduction of basal cell proliferation in Axl knockout mice also implies that instillation of a high volume of thymocytes per se does not affect basal cells indirectly.

Although other Axl-expressing cells do not appear to be present in the trachea at homeostasis, they may be recruited during influenza infection. Therefore we performed influenza virus infection in CCR2 knockout mice that are unable to release monocytes from the bone marrow (Boring et al., 1997). Without monocytes, their recruitment to the trachea, and differentiation into macrophages that might express Axl, is inhibited. In this system, basal cells still proliferated, often at greater levels than WT controls, which likely reflects the increased disease severity in this knockout mouse strain (Fig. 4).

An absence of Axl causes asymmetric basal cell division

Above, we showed that recognition of apoptotic cells via Axl causes basal cells to proliferate to produce more basal cells (symmetric division). However, murine basal cells also divide asymmetrically to replenish the multiple epithelial cell subsets in vivo (Paul et al., 2014). Asymmetric cell division, in which a single cell divides into two distinct cell types, is a biologically fundamental and evolutionally conserved process to generate a diversity of descendant cell types (Jan and Jan, 1998). Although intrinsic factors, such as oxidative stress pathways, regulate cell division symmetry in vitro (Paul et al., 2014), the extrinsic factors that control cell division symmetry in response to injury in vivo are undefined. We therefore asked whether Axl recognition of apoptotic cells influenced cell division symmetry under inflammatory conditions. To assess this, we measured the division angle of paired mitotic basal cells relative to basement membrane by immunofluorescence staining (Paul et al., 2014). Localization of survivin allows visualization of paired mitotic cells, since it is selectively expressed in the spindle midbody that appears in anaphase and telophase during mitosis (Williams et al., 2011). Fig. 5 A shows representative images of symmetric or asymmetric division of paired mitotic basal cells in the trachea 8 d after influenza infection. In symmetric division, basal cells divide horizontally to the basement membrane and display similar expression of the basal cell markers, TP63 and Krt5 (Fig. 5 A, upper panels). In contrast, in asymmetric division, basal cells divide vertically to the basement membrane resulting, in one TP63^{hi}/K5^{hi} basal cell on the basement membrane and above it (the other side of the spindle midbody) a TP63$^-$/K5^{low} cell that does not have the basal cell phenotype on the apical side (Fig. 5 A, lower panels). We sought to quantify this by plotting TP63 intensity ratio and cell division angle of each pair of survivin-positive mitotic basal cells and verified a significant correlation between these two parameters (Fig. 5 B). Generally, the lower the expression of TP63, the greater the division angle relative to the basement membrane (asymmetric division). *Axl*$^{-/-}$ mice displayed less TP63 intensity and had a greater division angle (Fig. 5 B). 48% of paired mitotic basal cells in WT C57BL/6 mice showed symmetric division (within 20° relative to the basement membrane), whereas only 26% of divisions were symmetric in *Axl*$^{-/-}$ mice 8 d after influenza infection (Fig. 5 C).

To further confirm that Axl regulates cell division symmetry, we used a three-dimensional (3D) organoid culture assay, which enables visualization of cell fates at the single-cell level ex vivo (Rock et al., 2011). As shown in Fig. S3, basal cells sorted from tracheas of WT or *Axl*$^{-/-}$ mice were cultured on top of

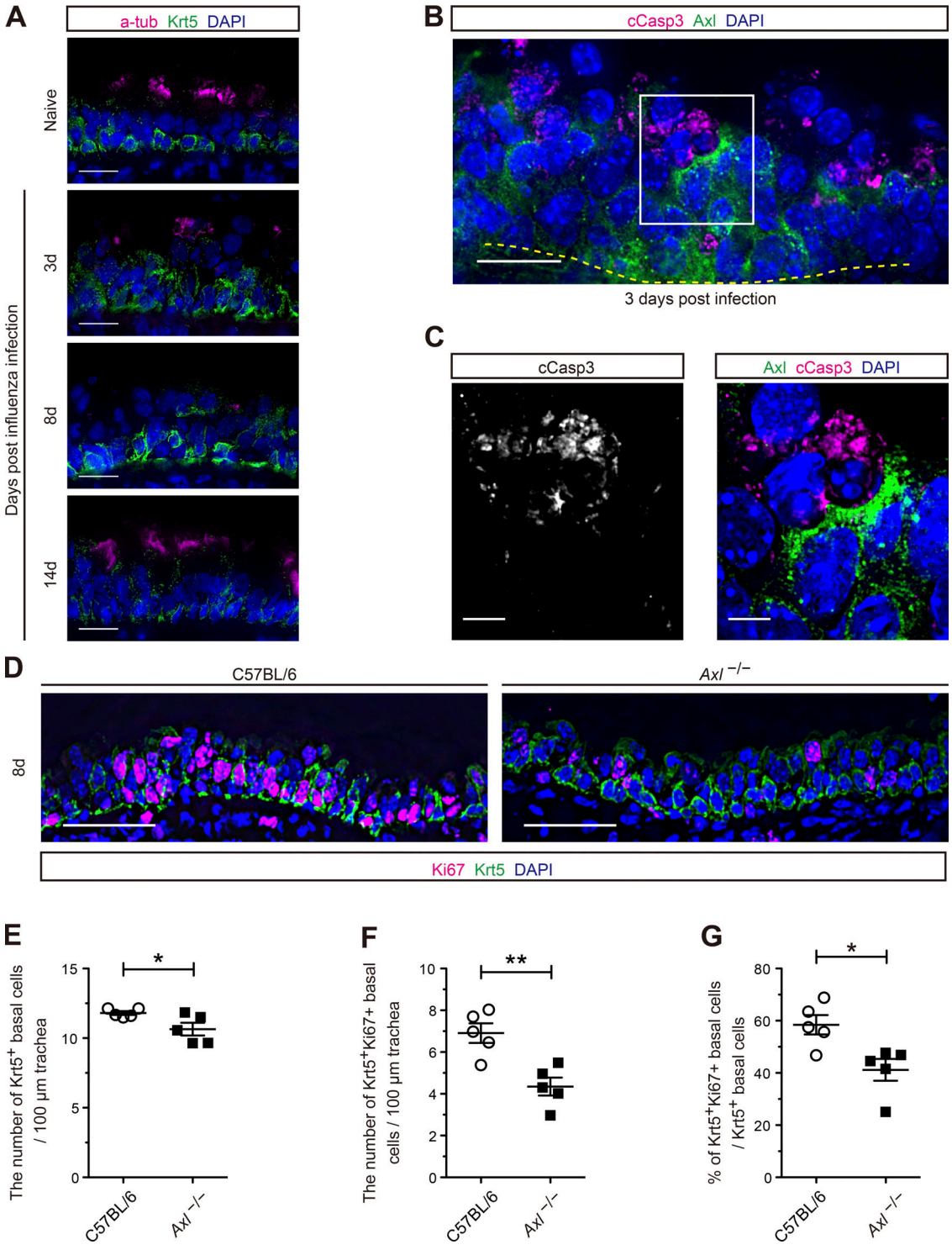

Figure 2. **Reduced cell cycle reentry of airway basal cells in *Axl*$^{-/-}$ mice in response to influenza virus–induced epithelial injury in vivo. (A)** Immunostaining of murine trachea epithelium for Krt5 (basal cell, green) and acetylated tubulin (a-tub; ciliated cell, magenta) after infection with H1N1/PR8 influenza A virus, confirming injury and repopulation of airway epithelium. **(B)** Immunofluorescent staining of cleaved caspase3 (cCasp3)–positive apoptotic cells (magenta) and their close contact with Axl^{+} cells (green). **(C)** Magnified views of the area indicated by white rectangle in B. **(D)** Murine trachea epithelium from C57BL/6 and *Axl*$^{-/-}$ mice after 8 d of influenza infection was stained for Ki67 (magenta) and Krt5 (green). **(E–G)** The number of Krt5^{+} basal cells per 100 µm trachea (E), the number of Krt5^{+}Ki67^{+} basal cells per 100 µm trachea (F), and the percentage of Krt5^{+}Ki67^{+} basal cells to total Krt5^{+} basal cells (G) between C57BL6 and *Axl*$^{-/-}$ mice 8 d after influenza inoculation. Data are combined from two independent experiments and are shown as mean ± SEM. *, P < 0.05; **, P < 0.01 vs. C57BL/6; two-tailed unpaired *t* test. Nuclei (blue) were stained with DAPI (A–D). Scale bars represent 10 µm (A and B), 5 µm (C), and 50 µm (D).

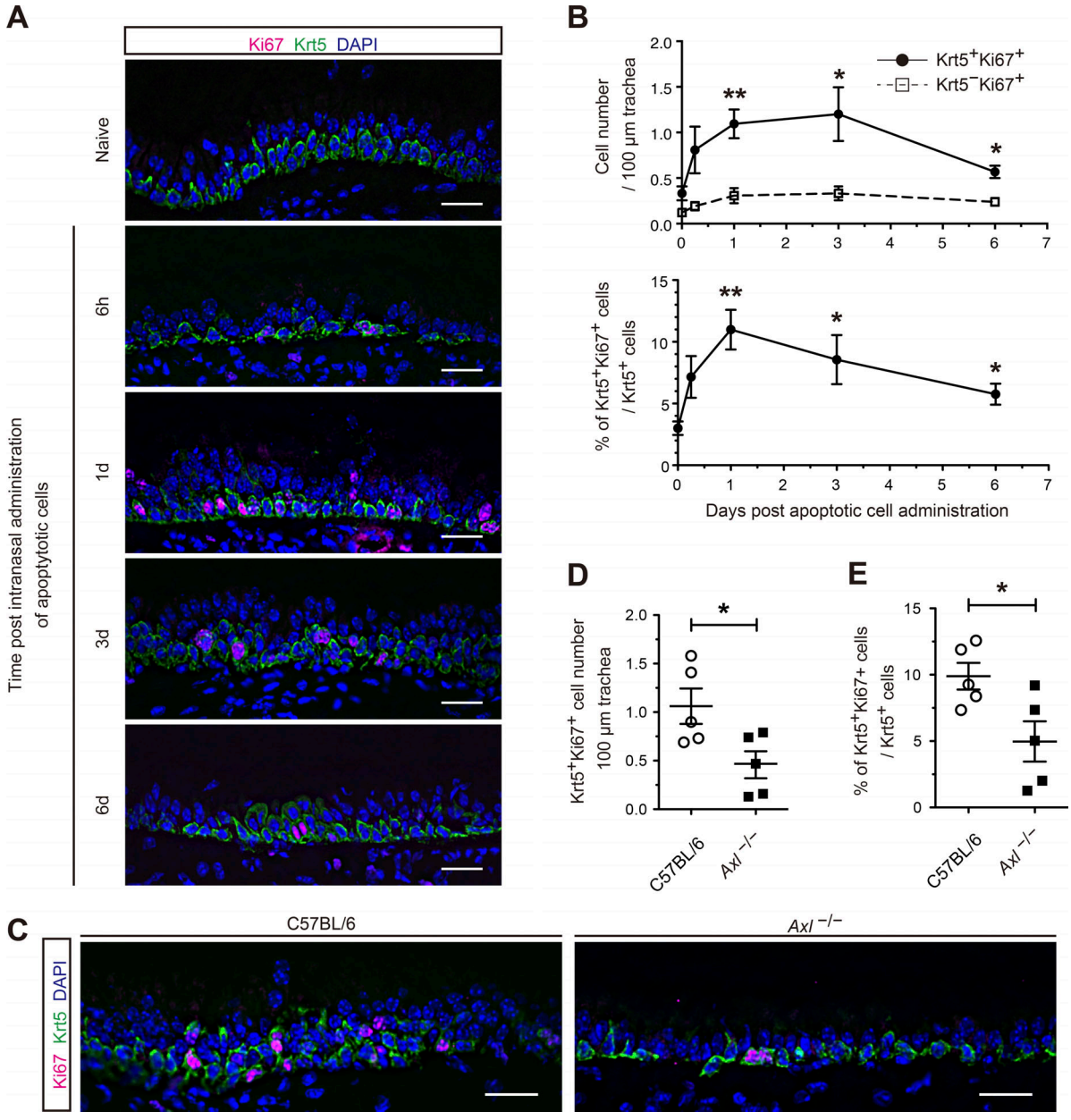

Figure 3. **Axl has an important role in apoptotic cell–triggered cell cycle reentry of airway basal cells in vivo. (A)** Immunostaining of murine tracheal epithelium for Ki67⁺ (magenta)/Krt5⁺ (green) basal cells in WT C57BL/6 mice after intranasal delivery of apoptotic thymocytes. **(B)** The number of Krt5⁺Ki67⁺ basal cells per 100 µm trachea (upper) and the percentage of Krt5⁺Ki67⁺ basal cells to total Krt5⁺ basal cells (lower) following intranasal administration of apoptotic thymocytes (0–6 d after administration). Data from one experiment with five mice per time point are expressed as mean ± SEM. *, P < 0.05; **, P < 0.01 vs. naive group (day 0); two-tailed unpaired *t* test. **(C)** Immunostaining of Ki67⁺ (magenta)/Krt5⁺ (green) airway basal cells in C57BL/6 and *Axl*$^{-/-}$ mice 1 d after intranasal administration of apoptotic thymocytes. **(D and E)** The number of Krt5⁺Ki67⁺ basal cells per 100 µm trachea (D) and the percentage of Krt5⁺Ki67⁺ basal cells to total Krt5⁺ basal cells (E) in *Axl*$^{-/-}$ mice compared with C57BL/6 mice 1 d after administration of apoptotic thymocytes. Data are representative of two independent experiments and are expressed as mean ± SEM of five individual mice. *, P < 0.05 vs. C57BL/6; two-tailed unpaired *t* test. Nuclei (blue) were stained with DAPI, and scale bars represent 20 µm (A and C).

extracellular matrices containing an Axl-activating antibody to fully activate the Axl signaling pathway. We observed 56 spheres from WT mice and 53 from *Axl*$^{-/-}$ mice at the two-cell stage and measured the TP63 intensity ratio of these two dividing cells (Fig. 5 D). This confirmed a significant decrease in basal cell–specific TP63 intensity ratio in spheres from *Axl*$^{-/-}$ mice compared with WT mice (Fig. 5 E). This suggests that Axl plays two roles: (i) in the presence of apoptotic cells, it promotes basal cell expansion by symmetric cell division, and (ii) an absence of Axl allows basal cell differentiation into other cell types by asymmetric cell division.

An absence of Axl promotes reepithelialization during influenza infection

If our theory is correct that Axl kinase promotes symmetric division of tracheal basal cells and inhibits their differentiation,

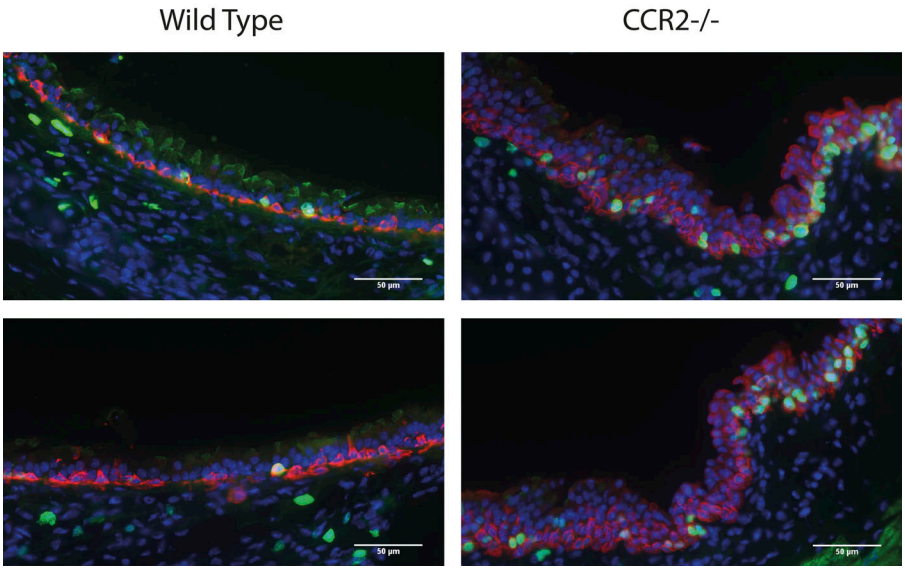

Figure 4. **Increased cell cycle reentry of airway basal cells in CCR2$^{-/-}$ airways following resolution of influenza virus infection.** Representative immunostaining of murine tracheal epithelium of C57BL/6 and CCR2$^{-/-}$ mice, for Ki67 (green), Krt5 (red), and nuclei (blue) at 14 d after H1N1/PR8 influenza A infection. Two representative images are shown for each mouse strain at 14 d after influenza virus infection. All images were obtained using 20× objective lens with scale bars, 50 µm.

then *Axl*$^{-/-}$ mice should exhibit accelerated ciliated cell repopulation after injury. To test this, we measured the area of cilia (acetylated tubulin–positive) in the trachea of mice infected with H1N1/PR8 influenza A virus. Although the area of cilia was equally reduced 3 d after infection in both WT and *Axl*$^{-/-}$ mice, we observed a significant increase in the cilia area in *Axl*$^{-/-}$ mice 8 d after infection (Fig. 6, A and B). We further confirmed this by demonstrating up-regulation of Foxj1 expression (a transcription factor selectively expressed by airway ciliated epithelial cells) in *Axl*$^{-/-}$ mice (a 1.8-fold increase in the ratio of Foxj1^{+} ciliated cells to K5^{+} basal cells/µm airway; Fig. 6, C and D). These data suggest that Axl is required to induce proliferation of basal cells and to suppress differentiation of basal cells into ciliated cells for reepithelialization.

An absence of Axl has long-term consequences on the tracheal epithelial barrier

We next examined how an absence of Axl affects the tracheal epithelial barrier at later time points after influenza infection. Before infection, the tracheal ciliated epithelium was indistinguishable between WT and *Axl*$^{-/-}$ mice. However, at later time points, particularly day 21, the epithelium appeared different in *Axl*$^{-/-}$ mice, with reduced cilia (Fig. 7, A–C), decreased epithelial thickness (Fig. 7 D), and a reduction in the number of nucleated cells (Figs. 7 E and S4). This implies that although epithelial barrier repair is faster in the absence of Axl, over the long term it is aberrant, and that these alterations are apparent only following epithelial cell death.

An increase in apoptotic cells is associated with proliferation of Axl^{+}/TP63^{+} basal cells in the airway of patients with COPD

So far, using murine models, we have demonstrated that sensing of apoptotic cells under inflammatory conditions initiates murine tracheal basal cell proliferation through Axl receptor tyrosine kinase. We further sought to confirm this idea in the human setting and explore clinical relevance to human airway inflammatory diseases. COPD is a common, preventable, and treatable disease characterized by persistent respiratory symptoms and airflow limitation due to airway and/or alveolar abnormalities, usually caused by significant exposure to noxious particles or gases (Vogelmeier et al., 2017). Aberrant proliferation and function of basal cells and an abnormal increase in apoptotic epithelial cells participate in the airway inflammation and obstruction seen in the pathogenesis of COPD (Hodge et al., 2005; Shaykhiev and Crystal, 2014b). Here we asked if human airway basal cells expressed Axl as with murine tracheal basal cells and evaluated how the presence of apoptotic cells was linked to Axl-expressing basal cells in airways of patients with COPD.

A transcriptome analysis of central, large-airway epithelial subsets previously revealed a sixfold increase in *AXL* mRNA expression of airway basal cells compared with differentiated luminal cells (Hackett et al., 2011). Here we wished to investigate Axl expression in the small airways (i.e., <2 mm internal diameter) in peripheral lung tissues, because small airways, but not large airways, are major sites of obstruction in patients with COPD (Hogg et al., 1968; Van Brabandt et al., 1983; Yanai et al., 1992). We used a monoclonal antibody against a cytoplasmic domain of Axl to prevent detection of the soluble form of Axl that is shed by inflammatory stimuli (Zagórska et al., 2014). The patient characteristics in our histological assessment are shown in Table 1. Unlike with ∼97% Axl expression on murine tracheal basal cells (Fig. 1 B), 24.4 ± 1.6% (mean ± SEM) of TP63^{+} basal cells expressed Axl in small-airway epithelium of control never-smokers (Fig. 8, A and B). The number and percentage of Axl^{+}/TP63^{+} basal cells were significantly increased in COPD ex-smokers compared with those in control never-smokers and control ex-smokers (Fig. 8, B and C). The number of Axl^{+}/TP63^{+} basal cells correlated with functional airway obstruction (i.e., disease severity; Fig. 8 D). Furthermore, Ki67-expressing Axl^{+}/TP63^{+} basal cells in the epithelium was observed only in COPD (Fig. 8, E and F), suggesting that the increase in the number of Axl^{+}/TP63^{+} basal cells in COPD was at least partially due to their proliferation. We next evaluated the presence of apoptotic cells using immunohistochemistry for cleaved caspase 3. We found a significant increase in cleaved caspase 3–positive

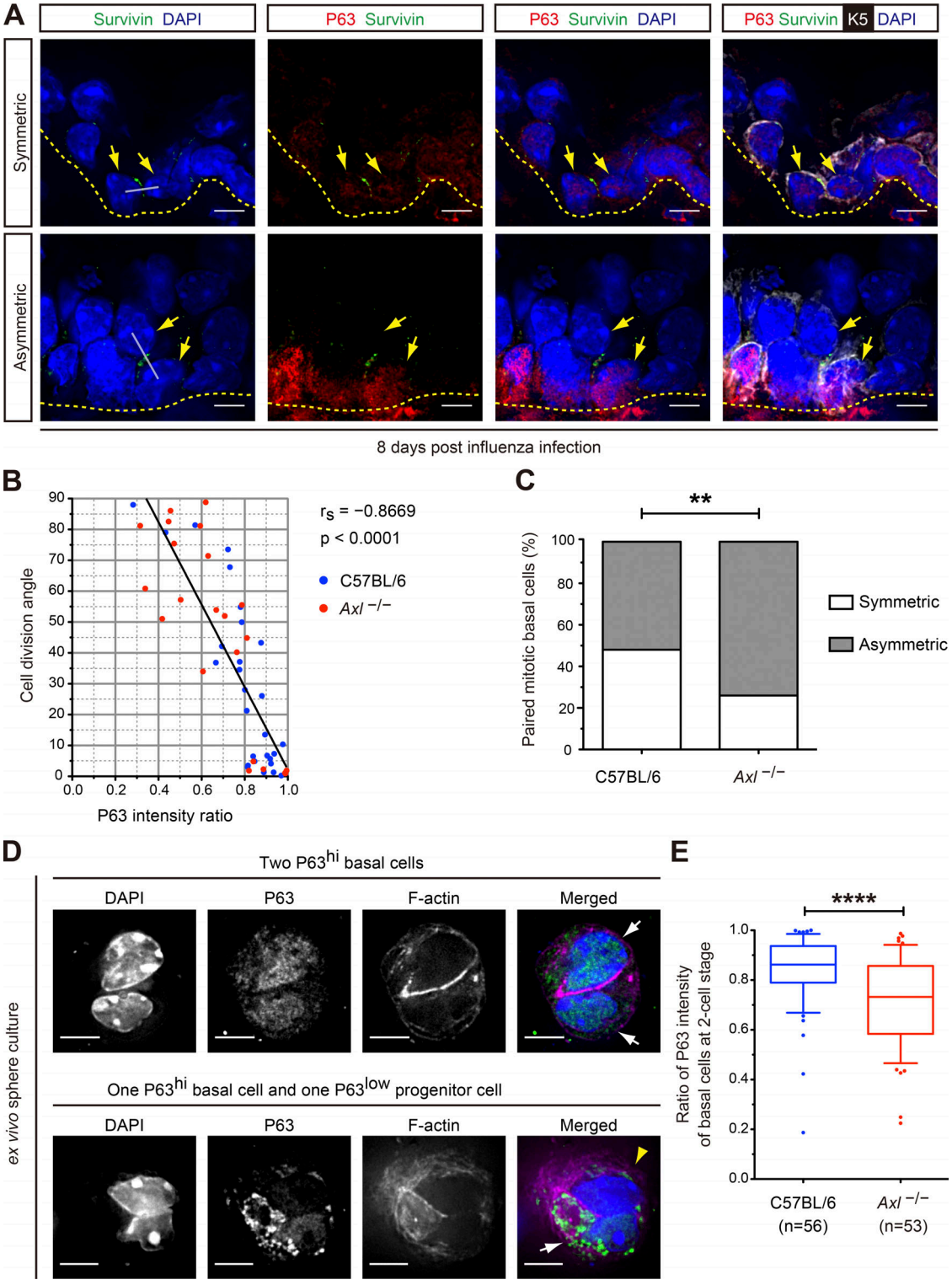

Figure 5. **Decreased symmetric division of airway basal cells in *Axl*$^{-/-}$ mice in response to influenza virus–induced epithelial injury in vivo and in a 3D organoid culture ex vivo. (A)** Representative examples of immunodetection of symmetric (top panels) and asymmetric (bottom panels) divisions in tracheas of C57BL/6 mice 8 d after H1N1/PR8 influenza virus infection; TP63 (red), Survivin (green), and Krt5 (K5; white). Yellow arrows indicate paired mitotic cells. Yellow dotted lines show basement membrane, and white faint lines on the left side panels indicate the direction of cell division. **(B)** Correlation of the TP63 intensity ratio and the cell division angle of each paired mitotic basal cell (n = 21 Axl$^{-/-}$ and 27 C57BL/6; Spearman's rank-order coefficient, r_s, = −0.8669, P < 0.0001). **(C)** Reduced symmetric division of basal cells in trachea in *Axl*$^{-/-}$ mice compared with C57BL/6, **, P = 0.0013; χ^2 test. Data in B and C are combined from two independent experiments with three individual mice per experiment. **(D)** Representative images of spheres at the two-cell stage consisting of a pair of P63^{hi} basal cells (white arrows, upper panels) or a TP63^{hi} basal cell (white arrow) with a TP63^{low} progenitor cell (yellow arrowhead; lower panels). TP63, green; F-actin, magenta; DAPI, blue. Scale bars represent 5 µm. **(E)** Axl-deficient basal cells show reduced the ratio of TP63 intensity at the two-cell stage. n = the number of spheres observed. Data are combined from two independent experiments and are expressed as box-and-whiskers plot (error bars indicate 10th to 90th percentile). Outliers are shown as dots. ****, P < 0.0001 vs. C57BL/6, Mann–Whitney U nonparametric test.

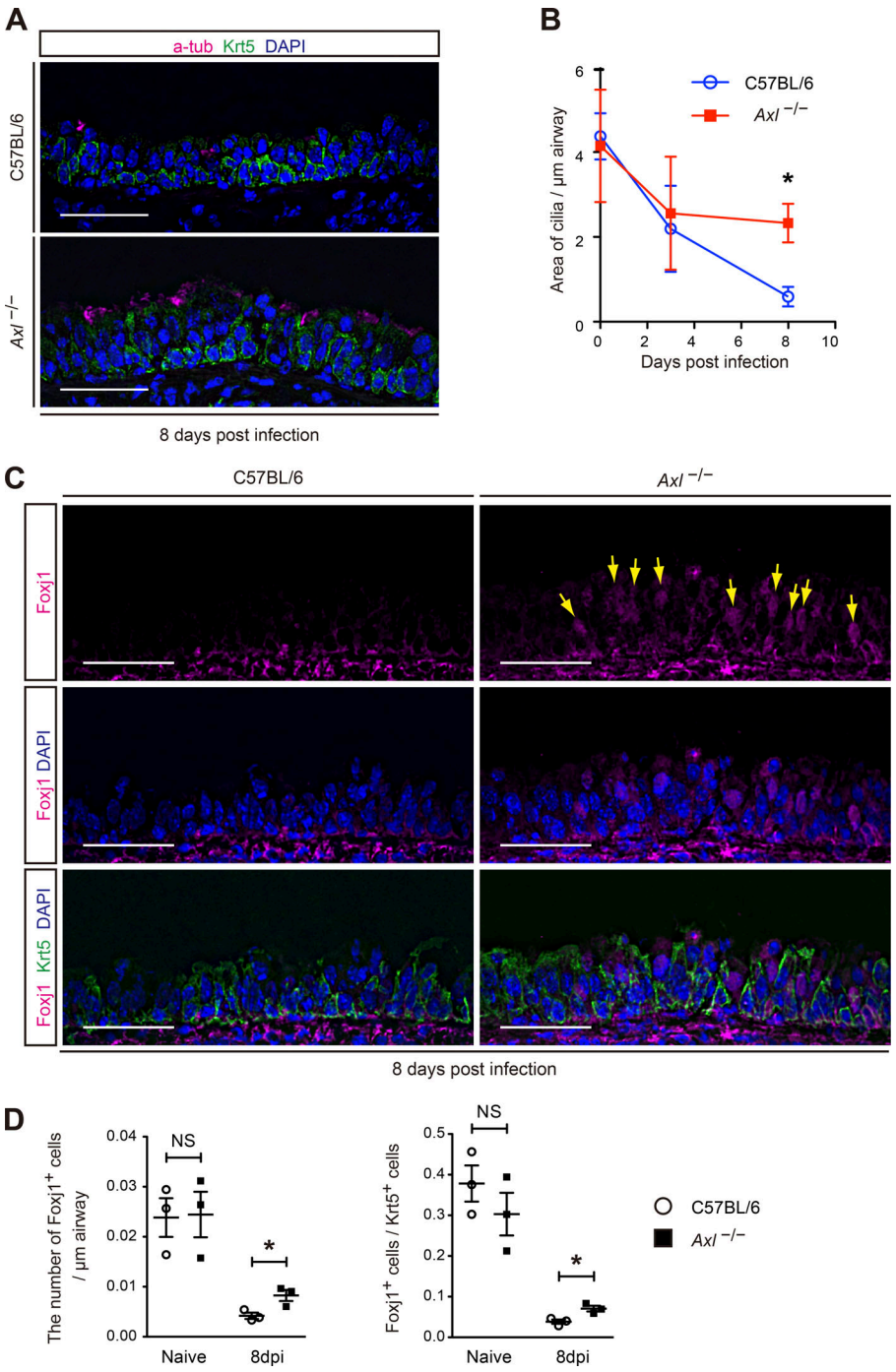

Figure 6. **Ciliated cell regeneration is promoted in *Axl*$^{-/-}$ mice at an early phase of influenza virus–induced epithelial injury in vivo. (A)** Immunostaining of cilia (acetylated tubulin, magenta) and basal cells (Krt5, green) of mouse tracheas at day 8 after H1N1/PR8 influenza A virus infection. **(B)** Quantification of area covered by cilia/µm of airways. **(C)** Immunostaining of ciliated cells (Foxj1, magenta) and basal cells (Krt5, green) of mouse tracheas 8 d after infection of C57BL/6 or Axl-deficient mice. Yellow arrows indicate nuclear staining of Foxj1 in ciliated cells. **(D)** Quantification of the number of Foxj1$^+$ ciliated cells/µm of airways (left graph) and the ratio of Foxj1$^+$ cells to Krt5$^+$ basal cells (right graph). Data are representative of two independent experiments and are expressed as mean ± SEM of three individual mice (B and D). *, $P < 0.05$ vs. C57BL/6; two-tailed unpaired *t* test. Nuclei (blue) were stained with DAPI, and scale bars represent 25 µm (A and C).

apoptotic cells in airway epithelium of COPD ex-smokers compared with control never-smokers and control ex-smokers (Fig. 8, G and H). We also found that the abundance of apoptotic cells was significantly correlated with functional airway obstruction (Fig. 8 I). Finally, this increase in caspase 3–positive apoptotic cells was significantly correlated with Axl$^+$/TP63$^+$ basal cells or Ki67$^+$/Axl$^+$/TP63$^+$ proliferating basal cells (Fig. 8, J and K).

Discussion

We demonstrate here that apoptotic cells are associated with cell cycle reentry of quiescent basal cells via Axl in inflammatory lung diseases of mice and humans. The outcome is symmetric cell division that increases the pool of proliferating basal cells. However, to drive basal cell differentiation to ciliated epithelial cells requires an absence of Axl. This approach is beneficial, as repair of an epithelial barrier, while there is ongoing stress leading to its apoptosis, would expend fruitless energy; differentiation may therefore progress once Axl signaling has ceased. The outcome of Axl signaling in basal cells fits with the early pathological changes observed in a number of chronic lung diseases. For example, defects in apoptotic cell clearance (Schmidt and Tuder, 2010), predominantly by airway macrophages (McCubbrey and Curtis, 2013; Grabiec and Hussell, 2016)

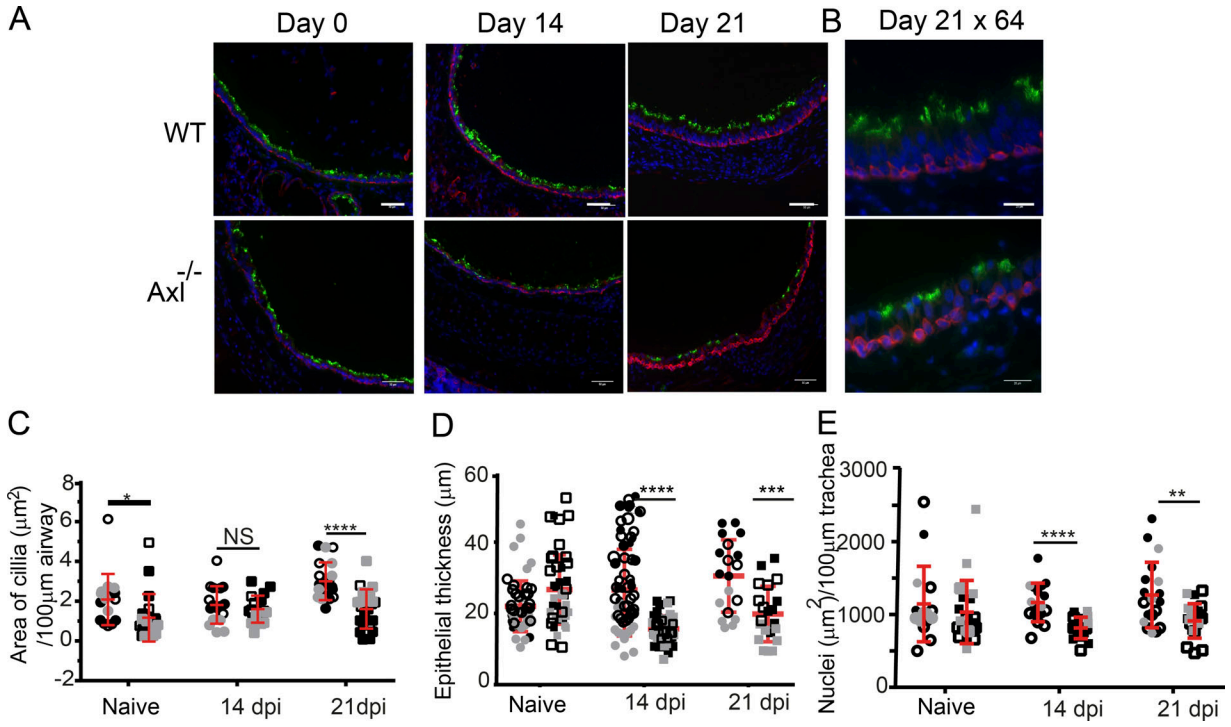

Figure 7. **Epithelial repair in *Axl*$^{-/-}$ mice is defective following the resolution of influenza viral infection. (A and B)** Representative images of immunostaining from murine trachea epithelium from C57BL/6 (WT) and *Axl*$^{-/-}$ mice for cilia (acetylated tubulin, green), basal cells (Krt5, red), and nuclei (blue) at day 0, 14, and 21 after H1N1/PR8 influenza A virus infection. Scale bars represent 50 µm. **(B)** Increased magnification (64×) of tracheal epithelium in the same region as shown in A of mice tracheas at day 21 after influenza virus infection. Scale bars represent 25 µm. **(C)** Quantification of area covered by cilia/µm of airways. **(D)** Quantification of epithelial thickness (µm) in the airways. **(E)** Quantification of epithelial surface area (basal cells to cilia) covered by nuclei (µm^2) per 100 µm of airway. Data are representative of mean (± SD) from three donors per condition. Each donor is identified by a different color (solid black, white with black border, and solid gray). C57BL/6 mice are indicated by circles, and *Axl*$^{-/-}$ mice are indicated by squares. Each symbol represents one field of view. *, P < 0.05; **, P < 0.01; ***, P < 0.001; ****, P < 0.0001, Mann–Whitney *U* nonparametric test.

are observed in cystic fibrosis (Vandivier et al., 2009), idiopathic pulmonary fibrosis (Morimoto et al., 2012), and COPD (Imai et al., 2005; Demedts et al., 2006; Makris et al., 2009). Furthermore, one of the earliest events in the development of COPD is basal cell hyperplasia (Auerbach et al., 1961) and a change in their transcriptome as disease develops (Crystal, 2014; Ryan et al., 2014; Shaykhiev and Crystal, 2014b). An increase of proliferating cells with basal cell–like features (cytokeratin 5/14–positive, EGFR$^+$) is also reported within the epithelium of cystic fibrosis patients compared with controls (Voynow et al., 2005).

Table 1. **Patient characteristics in the histological analysis**

Characteristic	Control never-smokers	Control ex-smokers	COPD ex-smokers
Subjects (*n*)	8	10	11
Men/women	0/8	8/2[a]	8/3[a]
Age (yr)	71.1 ± 6.6	69.0 ± 10.2	70.1 ± 7.7
Smoking (pack/yr)	0.0 ± 0.0	37.5 ± 27.2[a]	53.2 ± 33.1[b]
FVC (% of predicted)	106.1 ± 15.6	105.0 ± 11.7	106.0 ± 13.4
FEV_1 (% of predicted)	108.4 ± 16.0	114.1 ± 20.2	75.5 ± 14.9[a,c]
FEV_1/FVC (%)	78.3 ± 7.0	81.1 ± 8.0	55.7 ± 10.2[a,c]
GOLD (I/II/III/IV)			4/7/0/0

Data are presented as mean ± SD. FVC, forced vital capacity; FEV_1, forced expiratory volume in 1 s; GOLD, Global Initiative for Chronic Obstructive Lung Disease.
[a]P < 0.01.
[b]P < 0.001 vs. control never-smokers.
[c]P < 0.001 vs. control ex-smokers.

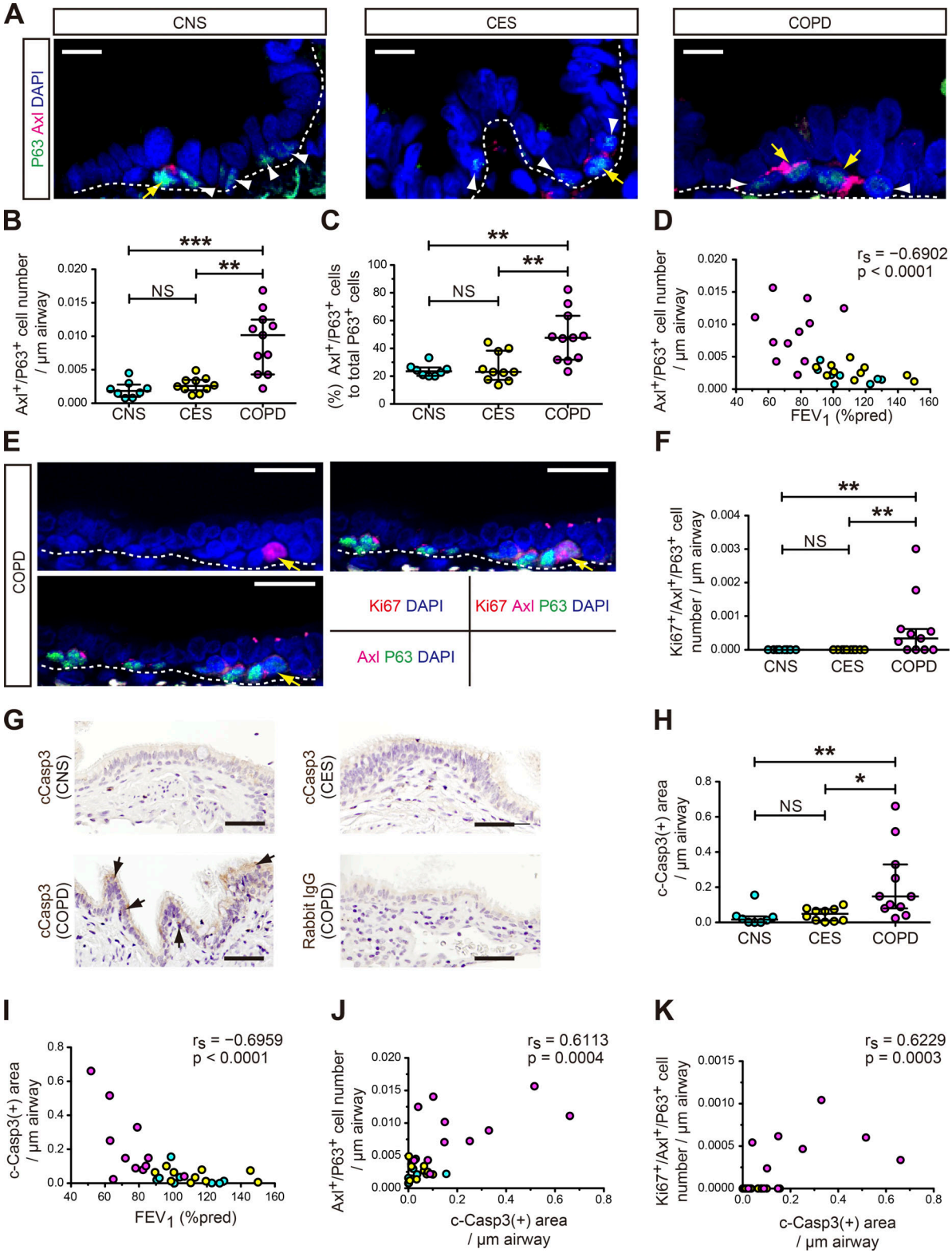

Figure 8. **Proliferation of Axl-expressing basal cells is correlated with the abundance of apoptotic cells in small airways of patients with COPD. (A)** Immunostaining of human small airway epithelium for P63 (a basal cell marker, green) and Axl (magenta) in control never-smokers (CNS), control ex-smokers (CES), and ex-smokers with COPD. Yellow arrows or white arrowheads indicate $Axl^+/TP63^+$ cells or $Axl^-/TP63^+$ cells, respectively. Dotted lines show basement membranes. **(B and C)** Quantification of the number of Axl-expressing $TP63^+$ basal cells/µm airway (B) and the percentage of Axl-expressing $TP63^+$ basal cells to total $TP63^+$ basal cells (C) in CNS, CES, and COPD. **(D)** Correlation between $Axl^+/TP63^+$ cell number/µm airway and airflow limitation detected as forced expiratory volume in 1 s (FEV_1, %pred). **(E)** Immunostaining for Ki67 (red), TP63 (green), and Axl (magenta) in small airways of COPD lung tissues. Yellow arrows indicate $Ki67^+/Axl^+/TP63^+$ cells. Dotted lines show basement membranes. **(F)** The increase in the Ki67-expressing $Axl^+/TP63^+$ basal cells in COPD compared

with CNS and CES. **(G)** Immunohistochemistry of cleaved caspase 3 (cCasp3, brown, arrows) in bronchiolar epithelium of human lung tissues from CNS, CES, and COPD. Nuclei (purple) were visualized by hematoxylin. **(H)** Quantification of cCasp3-positive area/µm of airways. **(I)** Correlation between cCasp3-positive area/µm of airways and FEV_1, %pred. **(J and K)** cCasp3 positivity is correlated with the number of $Axl^+/P63^+$ cell number (J) and $Ki67^+/Axl^+/TP63^+$ cell number in human small airway (K). Nuclei (blue) were stained with DAPI (A and E). Scale bars represent 25 µm (A and E) and 50 µm (G). Data are expressed as median ± interquartile range; Kruskal–Wallis test followed by Dunn's multiple comparison test, *, $P < 0.05$; **, $P < 0.01$; ***, $P < 0.001$ (B, C, and H). r_s, Spearman's rank-order coefficient (D, F, and I–K).

Our results would suggest that apoptotic cell excess and basal cell proliferation might be linked via the expression of Axl.

A role for Axl in barrier repair is supported further by our previous study showing that inhibition of Axl in vitro, using a small molecule inhibitor or by siRNA in human lung-derived multipotent cells, promotes epithelial cell traits including an up-regulation of surfactant proteins. Conversely, the presence of Axl controls a number of transcription factors associated with epithelial-to-mesenchymal transition such as SNAI2, HOXA5, TBX2, or TBX3 (Fujino et al., 2017). This raises the intriguing possibility that Axl acts as a switch to repair epithelial barriers at various levels of the respiratory tract. The current article drives the extension of this concept into a whole-animal model, where we identify traits relevant to several significant inflammatory diseases. However, in the in vivo model, although we can infer a direct effect of apoptotic cells on Axl-bearing basal cells, we cannot entirely rule out an indirect effect on another epithelial cell population.

In addition to basal cell hyperplasia and the presence of excess apoptotic cells, inflammatory lung diseases display a disordered airway epithelial barrier with shorter or absent cilia, loss of cell junctions, excess mucus, and squamous metaplasia (Auerbach et al., 1961; Kennedy et al., 1984; Lumsden et al., 1984; Peters et al., 1993; Dye and Adler, 1994; Leopold et al., 2009; Shaykhiev et al., 2011; Shaykhiev and Crystal, 2014a). Only 44% of basal cells from smokers differentiate to a mucociliated epithelium at air–liquid interface, compared with 88% from healthy nonsmokers (Staudt et al., 2014). In addition to the continued influence of noxious substances, the disordered epithelium may arise because Axl on basal cells promotes their proliferation and not their differentiation. Additionally, we show here that although ciliated airway epithelial cells are restored faster in Axl knockout mice compared with WT mice in response to injury, the resultant barrier is thinner, with shortened cilia. An abnormal but complete epithelial barrier may therefore be common across multiple respiratory diseases.

An important question is why this situation arises, and we believe the answer lies in how the system is alerted to the presence of damage. In the lung, antigen alone rarely leads to inflammation unless it is accompanied by structural damage. Various cell types sense tissue damage by recognizing "misplaced" proteins such as damage-associated molecular patterns including heat shock proteins, ATP, nucleosomes, mitochondrial proteins, and alarmins (Seong and Matzinger, 2004; Bertheloot and Latz, 2017). Such damage-associated molecular patterns are kept to a minimum by the antiinflammatory process of apoptosis. However, it would also be important for a system to sense that excessive apoptotic cell turnover was occurring. We propose that apoptotic cells perform a function similar to an alarmin that promotes basal cell activity to replace damaged epithelium once apoptosis has ceased. The fact that basal cell hyperplasia is not observed in health suggests that homeostatic apoptotic cell turnover is not a sufficient signal in this process. Basal cell proliferation may therefore depend on the extent of Axl ligation and/or require additional microenvironmental cues (Arandjelovic and Ravichandran, 2015). In addition to externalized phosphatidylserine, apoptotic cells also express on their cell surface ICAM-3, oxidized low-density lipoprotein, calreticulin, annexin 1, thrombospondin, and C1q. However, these do not compensate for a lack of Axl in driving basal cell proliferation, which highlights a surprising specificity of Axl's effect.

That Axl is constitutively expressed on basal cells raises the question of how Axl activity in this context is regulated. Basal cells are usually shielded from the airway lumen by other epithelial cells, and interstitial lung contents by the basement membrane. In acute and chronic inflammatory diseases, both of these shields are damaged in patches. Therefore, basal cell recognition of apoptotic cells by Axl is likely to occur only in patches. This is supported by the small localized areas of basal cell Ki67 staining that we observe by immunofluorescence during influenza infection. That instilled apoptotic cells also induced basal cell proliferation is interesting, as this process is unlikely to denude epithelial cells. Phosphatidylserine-coated exosomes released from cells that are small enough to transit into the epithelial barrier may be present in this scenario (Arraud et al., 2015). Another conundrum is that we might expect progressive depletion of basal cells in Axl knockout mice, since it is required for basal cell cycle reentry during inflammation. There are currently two explanations for why basal cells are not depleted in Axl knockout mice. First, homeostatic turnover of basal cells is likely to be Axl independent due to the paucity of apoptotic cells, and second, basal cells in nondamaged areas of epithelium may compensate through symmetric cell division.

Phosphatidylserine is expressed in the virion coat of a number of viruses and may facilitate virus entry through phosphatidylserine-recognizing receptors. The outcome of this route of infection is critical for determining whether the virus then replicates or not. The human T cell immunoglobulin and mucin domain proteins have been extensively studied in this regard (Mercer and Helenius, 2008; Soares et al., 2008), but Axl is also involved due to the binding of its bridging ligand, Gas6, to phosphatidylserine. Alhough H1N1 influenza virus has not been studied in this respect, H7N1 virus entry via this route leads to a nonproductive infection (Jemielity et al., 2013). This, along with the observation of major changes in the barrier epithelium long after the virus has been cleared, suggests that viral entry into basal cells is not a predominant cause of our results.

Axl therefore contributes to significant clinical features associated with inflammatory lung disease, including basal cell hyperplasia and disrupted epithelial basement membrane. This suggests that Axl inhibition may be beneficial in a variety of inflammatory lung disease settings. In this regard, therapeutics are already in clinical trials, as members of the TAM receptor family are aberrantly or ectopically expressed in many hematologic and nonhematologic malignancies, where they contribute to increased cell survival and proliferation, thereby increasing resistance to chemotherapeutics and targeted agents (Graham et al., 2014; Akalu et al., 2017). The tyrosine kinase inhibitors, ligand traps, and monoclonal antibodies already developed could therefore be repurposed for chronic inflammatory diseases such as COPD, which itself is associated with eventual development of lung cancer.

Materials and methods

Mice

The generation of *Axl*$^{-/-}$ mice has been described previously (Lu et al., 1999). All *Axl*$^{-/-}$ mice used in this study were backcrossed to C57BL/6J background for ≥10 generations. C57BL/6J littermates were bred in-house and used as controls and Ccr2^{tm1Ifc} (Boring et al., 1997). All experiments were approved under a project license granted by the Home Office UK and by the University of Manchester Animal Welfare and Ethical Review Body and were performed in accordance with the UK Animals (Scientific Procedures) Act of 1986. Mice were bred and maintained in specific pathogen–free conditions at Bio Safety Level 2 with a 12-h light/dark cycle, dry food pellets, and water ad libitum. 8–10-wk-old female mice were used for all in vivo experiments. 12–14-wk-old male and female mice were used for ex vivo culture assays.

Immunofluorescence staining and image analysis on mouse tissues

For dissection of tissues, mice were euthanized by intraperitoneal administration of 3 mg pentobarbitone and exsanguination via the femoral artery. Tracheas, lungs, and testes were harvested, embedded in optimal cutting temperature medium, and frozen in 2-methylbutane with dry ice. The tissues were sectioned in a Cryostat at 10-µm thickness, and tracheas were cut longitudinally. Sections were air-dried for 10 min and stored at −80°C. For immunofluorescence staining, sections were fixed with 4% paraformaldehyde for 30 min, blocked with 10% donkey serum/0.3% Triton X-100 in PBS for 30 min, and incubated at 4°C overnight with the following primary antibodies: rabbit anti-Krt5 (#905501, 1 µg/ml; BioLegend); chicken anti-Krt5 (#905901, 1 µg/ml; BioLegend); rabbit anti-P63 (ab124762 [EPR5701], 3.3 µg/ml; Abcam); mouse anti-P63 (ab735 [4A4], 1/100; Abcam); goat anti-Axl (AF854, 4 µg/ml; R&D Systems); goat anti-Mertk (BAF591, 4 µg/ml; R&D Systems); goat anti-Tyro3 (AF759, 4 µg/ml; R&D Systems); goat anti-Gas6 (BAF986, 4 µg/ml; R&D Systems); rat anti-Ki67 (#13-5698 [SolA15], 2.5 µg/ml; eBioscience); rabbit anti–acetylated tubulin (#5335 [D20G3], 1/800; Cell Signaling Technology); mouse anti-Foxj1 (#14-9965 [2A5], 1 µg/ml; eBioscience); rabbit anti-cleaved caspase 3 (#9664 [5A1E], 1/800; Cell Signaling Technology); and rabbit anti-survivin (#2808 [71G4B7], 1/400; Cell Signaling Technology). Mouse on Mouse Basic Kit (#BMK-2202; Vector) was used for mouse-derived primary antibodies per the manufacturer's instructions. After three washes for 5 min with PBS containing 0.02% Tween 20, the following fluorochrome-conjugated secondary antibodies were used: tetramethylrhodamine (TRITC)-donkey anti-rabbit IgG (711-025-152; Jackson ImmunoResearch), Alexa Fluor 647–donkey anti-goat IgG (705-605-147; Jackson ImmunoResearch), Alexa Fluor 488–donkey anti-chicken IgY (703-545-155; Jackson ImmunoResearch), Alexa Fluor 546–donkey anti-rabbit IgG (A10040; Life Technologies), Alexa Fluor 546–donkey anti-mouse IgG (A10036; Life Technologies), Alexa Fluor 488–donkey anti-goat IgG (A11055; Life Technologies) or fluorochrome-conjugated streptavidin (Alexa Fluor 488–Streptavidin (S11223; Life Technologies), and Alexa Fluor 647–Streptavidin (S21374; Life Technologies). Slides were mounted and nuclei were stained using ProLong Diamond antifade reagent with DAPI (Life Technologies).

Images were collected on an Olympus BX51 upright microscope using a 20×/0.50 Plan Fln or 40×/0.75 Plan Fln objective and captured using a Coolsnap ES camera (Photometrics) through MetaVue Software (Molecular Devices). Specific bandpass filter sets for DAPI, FITC, TRITC, and Cy5 were used to prevent bleed-through from one channel to the next. Deconvolved images were acquired on a Delta Vision (Applied Precision) restoration microscope using a 40×/1.30 Uplan Fln objective and the Sedat filter set (Chroma 86000v2). The images were collected using a Coolsnap HQ (Photometrics) camera with a Z optical spacing of 0.2 µm. Raw images were then deconvolved using Softworx software. Images were processed and analyzed using ImageJ, and median-intensity projections of the deconvolved images are shown.

For quantification, three independent sections from each trachea were examined by referencing cartilage rings 2–9 according to a previous publication (Tata et al., 2013). Cells that expressed each specific marker were manually counted. Cell division axis was determined in pairs of mitotic basal cells in anaphase or telophase by survivin staining (Williams et al., 2011). Cell division angle was defined as the angle between the division axis to the basement membrane. The ratio of TP63 staining intensity of paired mitotic basal cells was quantified using ImageJ as follows: (i) the outline of nuclei was delineated by DAPI staining; (ii) the average intensity of TP63 staining within the nucleus was measured and defined as TP63 intensity; (iii) the ratio of TP63 intensity of paired mitotic cells was calculated by dividing TP63 intensity of one daughter cell ($TP63_{Cell1}$) by TP63 intensity of another daughter cell ($TP63_{Cell2}$), where $TP63_{Cell2}$ is always greater than $TP63_{Cell1}$. The area of cilia, which were visualized by positivity of acetylated tubulin in tracheal epithelium, and the length of basement membrane were measured using ImageJ.

Isolation of murine tracheal cells

Murine tracheal cells were isolated using a Papain Dissociation System per the manufacturer's instructions (Worthington) and previous reports (Tata et al., 2013; Zhao et al., 2014). Briefly,

tracheas were cut into small pieces and incubated with papain solution at 37°C for 1.5 h and serially passed through 19-, 21-, and 23-gauge needles. The suspension of cells was subsequently filtered via a 70-µm cell strainer. Ovomucoid inhibitor solution contained in the Papain Dissociation System was used to inhibit the enzymatic activity of the papain solution, and debris was removed by discontinuous density gradient. RBCs were lysed with RBC lysis buffer (Roche).

FACS of epithelial cells from murine tracheas

Epithelial cell subsets were sorted from murine tracheas as described previously (Tata et al., 2013; Zhao et al., 2014). Briefly, single-cell suspensions were stained with Live/Dead Fixable Near-IR Dead Cell Stain Kit (Life Technologies) per the manufacturer's instructions. Fc receptors were then blocked using purified anti-mouse CD16/CD32 (14-061-85 [clone 93], 1:100; eBioscience) at 4°C for 20 min. Cells were stained with the following cocktail of antibodies and lectin in sterilized PBS containing 1% BSA at 4°C for 30 min: PE-anti-mouse CD326 (EpCAM) antibody (118205, 1:100; BioLegend); PE/Cy7-anti-mouse CD24 antibody (560536, 1:200; BD PharMingen); biotinylated *Griffonia simplicifolia* isolectin (GSI)-β4 (L2140, 1:100; Sigma-Aldrich); Alexa Fluor 647–anti-mouse/human CD15 (SSEA-1) antibody (125608, 1:50; BioLegend). The samples were then incubated with Brilliant Blue 515–conjugated streptavidin (564453, 1:100; BD Biosciences) at 4°C for 30 min to detect biotinylated GSI-β4. Cells were sorted using BD Influx. FlowJo (version 10) was used for FACS analysis.

RNA extraction, RT, and qPCR

Total RNA was extracted using RNeasy Micro Kit (Qiagen) and assessed for quantity and quality by UV spectrophotometry (ND-2000 spectrophotometer; Nano Drop Technologies). cDNA was synthesized from the extracted RNA using High-Capacity RNA-to-cDNA Kit (Life Technologies). qPCR was performed using the predesigned TaqMan expression assays and TaqMan Fast Universal PCR Master Mix (Life Technologies) on a QuantStudio 12K Flex PCR system (Life Technologies) in duplicate. The TaqMan expression assays used were *Hprt*, Mm01545399_m1; *Trp63*, Mm00495793_m1; *Scgb3a2*, Mm00504412_m1; *Foxj1*, Mm01267279_m1; and *Axl*, Mm00437221_m1. *Hprt* was used as the endogenous control, and relative expression of mRNA was determined by the ΔΔCt method.

Infection of influenza virus and EdU administration

Mice were anesthetized with isoflurane and intranasally infected with 7.5 PFU of H1N1 influenza A virus, Puerto Rico/8/34 (PR8). EdU (0.5 mg/200 µl PBS per mouse; Life Technologies) was intraperitoneally injected on days 3, 5, and 7 after influenza infection. Mice were euthanized by intraperitoneal administration of 3 mg pentobarbitone and exsanguination via the femoral artery on day 8. Tracheas were harvested for subsequent experiments.

Intranasal administration of apoptotic thymocytes

For preparation of apoptotic or necrotic thymocytes, thymi were harvested from 6–7-wk-old female C57BL/6 mice. Apoptotic cells were obtained by incubation of thymocytes with 2.5 µM dexamethasone for 5 h. Mice were anesthetized with isoflurane and intranasally administered with 50 µl of 0.8 mM $CaCl_2$/PBS containing 1.0 × 10^7 apoptotic cells.

Cell culture, whole-mount staining, and image analysis of a 3D basal cell organoid assay

3D basal cell organoids were generated as previously described (Rock et al., 2011) with some modification. Permanox 8-well chamber slides (Corning) were coated with Matrigel (10 µl/well; Corning) on ice using an ice-cold tip and incubated at 37°C for 10 min. $EpCAM^+GSI\text{-}β4^+CD24^-$ basal cells sorted from murine trachea were seeded at 5,000 cells/well onto slides precoated with 300 µl/well of mTEC/Plus medium (You et al., 2002) containing 2% Matrigel and anti-Axl–activating antibodies (AF854, 3 µg/ml at final concentration; R&D Systems). On day 1, 150 µl of culture supernatant per well was removed, and 150 µl/well mTEC/Plus medium containing the anti-Axl–activating antibody was added. On day 2, slides were fixed with 4% paraformaldehyde at room temperature for 30 min. Basal cell spheres were blocked and permeabilized with PBS containing 10% goat serum (Sigma-Aldrich) and 0.3% Triton X-100 for 30 min. An anti-P63 antibody (ab124762 [clone EPR5701]; Abcam) in blocking buffer was incubated overnight at 4°C. After rinsing slides with PBS containing 0.02% Tween20, the slides were incubated with Alexa Fluor 647–conjugated goat anti-rabbit antibody (Life Technologies) in 2% goat serum/PBS for 60 min. After incubation with Alexa Fluor 555–conjugated phalloidin for 20 min, slides were mounted, and nuclei were stained using ProLong Diamond antifade reagent with DAPI (Life Technologies). Deconvolved image acquisition using Delta Vision and image analysis for measuring TP63 intensity ratio were performed as described above.

Ex vivo proliferation assay of murine airway basal cells

Sorted basal cells were cultured on a 96-well view plate (#6005225; PerkinElmer) coated with rat tail collagen I (5 µg/cm^2; Corning) in DMEM (Sigma-Aldrich) containing 10 µg/ml insulin (Sigma-Aldrich), 5 µg/ml transferrin (Sigma-Aldrich), 0.1 µg/ml cholera toxin (Sigma-Aldrich), 2% bovine pituitary extract (Lonza), 5% FBS (Life Technologies), 0.01 µM retinoic acid (Sigma-Aldrich), 50 nM full-length mouse recombinant Gas6 (8310-GS; R&D Systems), 100 units/ml penicillin, 100 µg/ml streptomycin, and 0.25 µg/ml amphotericin B. 3 d after seeding, cells were fixed with 4% paraformaldehyde for 30 min. After a blocking/permeabilization step with 10% donkey serum/0.5% Triton X-100/PBS for 30 min, cells were incubated with biotinylated rat anti-Ki67 antibody (#13-5698 [SolA15], 2.5 µg/ml; eBioscience) overnight at 4°C. The cells were then incubated with Alexa Fluor 555–conjugated streptavidin for 15 min, and nuclei were stained with Hoechst 33342 (1 µg/ml at final concentration; Life Technologies) for 10 min. Images were acquired on a Leica DM IL LED inverted microscope using a 20×/0.35 Dry N Plan L objective and captured using a Leica DFC 3000G through Leica Application Suite Advanced Fluorescence software. Specific bandpass filter sets for DAPI and TRITC were used to prevent bleed-through from one

channel to the next. Images were processed and analyzed using ImageJ. At least 300 nuclei were manually counted in each well for calculating the percentage of Ki67$^+$ cells per total number of nuclei.

Human lung tissues and ethics

The study using human lung tissues was approved by the Ethics Committee at the Tohoku University School of Medicine and the Japanese Red Cross Ishinomaki Hospital. Lung tissues were obtained from patients who underwent lung resection for lung cancer at the Department of Thoracic Surgery at Tohoku University Hospital or the Department of Thoracic Surgery at Japanese Red Cross Ishinomaki Hospital. Written informed consent was received from all patients before surgery. Airflow limitation was determined by spirometry and was defined as a post-bronchodilator forced expiratory volume in 1 s/forced vital capacity <70%, and severity was classified in accordance with the Global Initiative for Chronic Obstructive Lung Disease criteria (Vogelmeier et al., 2017). Lung tissues distant from the cancerous lesions were used, and we verified that no tumors were included in sections analyzed by histopathology. We also confirmed that there was no overt inflammation and fibrosis in lung sections of control never-smokers and control ex-smokers.

Immunofluorescence staining and immunohistochemistry for human lung specimens

Lung tissues were fixed with 10% formalin, embedded in paraffin, and sectioned at 3-µm thickness. Heat-induced antigen retrieval by autoclave (for 5 min at 121°C) was performed using Tris-EDTA buffer (10 mM Tris base, 1 mM EDTA, and 0.05% Tween 20, pH 9.0). Triple immunofluorescence staining of Axl in combination with Ki67 and TP63 was performed. Sections were blocked and permeabilized for 30 min at room temperature with 0.3% Triton X-100/10% goat serum/PBS. The sections were incubated overnight at 4°C with primary antibodies as follows: anti-human Axl antibody (#8661, clone C89E7, rabbit monoclonal, 1:100; Cell Signaling Technology); anti-human TP63 antibody (#735, clone 4A4, mouse IgG2a, 1:100; Abcam); and anti-Ki67 antibody (#9449, clone 8D5, mouse IgG1, 1:200; Cell Signaling Technology). Secondary antibodies were incubated using Alexa Fluor 488–goat anti-mouse IgG2a antibody, Alexa Fluor 555–goat anti-rabbit IgG(H+L) antibody, and Alexa Fluor 647–goat anti-mouse IgG1 antibody (1:200; Thermo Fisher Scientific). After mounting of slides and staining of nuclei using ProLong diamond antifade reagent with DAPI (Life Technologies), images were collected on a Nikon C2si confocal microscope system using a 20×/0.75 Plan Apo or 60×/1.40 Plan Apo λ oil objective through NIS-Elements C (Nikon) with Z spacing of 0.150 µm. Images were processed and analyzed using NIS-Elements AR (Nikon), and maximum-intensity projections are shown.

Cleaved caspase 3 was stained using Histofine SAB-PO(R) kit (Nichirei) per the manufacturer's instructions. Briefly after heat-induced antigen retrieval using Tris-EDTA buffer as above, sections were blocked with 10% goat serum buffer. Anti-cleaved caspase 3 antibody (#9664, clone 5A1E, rabbit monoclonal, 1:1,000; Cell Signaling Technology) was incubated overnight at 4°C. After blocking endogenous peroxidase activity by incubating for 30 min at room temperature using methanol and 3% hydrogen peroxide, sections were incubated with biotinylated goat anti-rabbit antibody followed by streptavidin-conjugated horseradish peroxidase. 3,3′-Diaminobenzidine was used for detection of the antigen–antibody complex. Nuclei were visualized with hematoxylin. Images were acquired on an Olympus BX53 microscope using a 20×/0.50 UPlanFL N objective and captured using a DP71/u-TV1X-2 camera through a DP controller (Olympus). Images were processed and analyzed using ImageJ. For quantification, three small airways in each section were arbitrarily selected.

Statistical analysis

Prism version 5.0f (GraphPad Software) was used for all statistical calculations. For multiple dataset analysis, analysis of variance with Bonferroni correction was applied. To compare two datasets, unpaired *t* test or nonparametric Mann–Whitney *U* test was applied as indicated in figure legends. Fisher's exact test was used to test association between two categorical variables. To test correlation between two datasets, a Spearman rank-order correlation coefficient (r_s) and the P value were calculated. Data are presented as the mean ± SEM or SD as indicated in figure legends. P values <0.05 were considered significant.

Online supplemental material

Fig. S1 shows the sorting strategy and validation of cellular components in murine tracheal epithelium, the exclusive expression of Axl on basal cells, and the specificity of the anti-Axl antibody. Fig. S2 shows that the mouse trachea contains very few immune cells that express Axl. Fig. S3 shows details of how basal cell proliferation or differentiation was assessed. Fig. S4 shows that epithelial thickness and the number of nuclei are reduced in the absence of Axl.

Acknowledgments

We are grateful to Peter C. Cook and Gareth Howell (Manchester Collaborative Centre for Inflammation Research, the University of Manchester, Manchester, UK) for FACS; Takaya Suzuki, Takashi Kondo, Yoshinori Okada, and Chiharu Ota (Tohoku University, Sendai, Japan) and Satoshi Suzuki (Japanese Red Cross Ishinomaki Hospital, Miyagi, Japan) for obtaining human lung tissues. Special thanks go to Steve Mardsen for his help with the microscopy. We also thank the Biomedical Research Core of Tohoku University Graduate School of Medicine and the Biomedical Research Unit of Tohoku University Hospital for technical support.

This research was supported by a precompetitive open innovation award from AstraZeneca and GlaxoSmithKline that formed the Manchester Collaborative Centre for Inflammation Research. This work was also supported by the Japan Society for the Promotion of Science KAKENHI (grant nos. JP17H04180, JP16K15453, JP26293195, JP16H05307, and JP16H06641). The Bioimaging Facility microscopes used in this study were purchased with grants from Biotechnology and Biological Sciences Research Council, Wellcome Trust (grant no. 202865/Z/16/Z), and the University of Manchester Strategic Fund.

R.A. Maciewicz is an employee and shareholder of AstraZeneca. The other authors declare no competing financial interests.

Author contributions: N. Fujino conceived this project, designed strategy, performed experiments, analyzed/interpreted data, and wrote the manuscript. T. Fujimori conceived this project and performed in vivo experiments. O.J. Brand, D.J. Morgan, A.M. Grabiec, C.P. Jagger, and K. Itakura performed in vitro and in vivo experiments. R.A. Maciewicz conceived this project. M. Yamada, H. Sugiura, and M. Ichinose collected human samples and interpreted the data. T. Hussell conceived this project, designed strategy, interpreted data, and wrote the manuscript.

Submitted: 1 November 2017
Revised: 18 March 2019
Accepted: 14 June 2019

References

Akalu, Y.T., C.V. Rothlin, and S. Ghosh. 2017. TAM receptor tyrosine kinases as emerging targets of innate immune checkpoint blockade for cancer therapy. *Immunol. Rev.* 276:165–177. https://doi.org/10.1111/imr.12522

Arandjelovic, S., and K.S. Ravichandran. 2015. Phagocytosis of apoptotic cells in homeostasis. *Nat. Immunol.* 16:907–917. https://doi.org/10.1038/ni.3253

Arraud, N., C. Gounou, R. Linares, and A.R. Brisson. 2015. A simple flow cytometry method improves the detection of phosphatidylserine-exposing extracellular vesicles. *J. Thromb. Haemost.* 13:237–247. https://doi.org/10.1111/jth.12767

Asiedu, M.K., F.D. Beauchamp-Perez, J.N. Ingle, M.D. Behrens, D.C. Radisky, and K.L. Knutson. 2014. AXL induces epithelial-to-mesenchymal transition and regulates the function of breast cancer stem cells. *Oncogene.* 33:1316–1324. https://doi.org/10.1038/onc.2013.57

Auerbach, O., A.P. Stout, E.C. Hammond, and L. Garfinkel. 1961. Changes in bronchial epithelium in relation to cigarette smoking and in relation to lung cancer. *N. Engl. J. Med.* 265:253–267. https://doi.org/10.1056/NEJM196108102650601

Balasooriya, G.I., J.A. Johnson, M.A. Basson, and E.L. Rawlins. 2016. An FGFR1-SPRY2 Signaling Axis Limits Basal Cell Proliferation in the Steady-State Airway Epithelium. *Dev. Cell.* 37:85–97. https://doi.org/10.1016/j.devcel.2016.03.001

Bergmann, A., and H. Steller. 2010. Apoptosis, stem cells, and tissue regeneration. *Sci. Signal.* 3:re8. https://doi.org/10.1126/scisignal.3145re8

Bertheloot, D., and E. Latz. 2017. HMGB1, IL-1α, IL-33 and S100 proteins: dual-function alarmins. *Cell. Mol. Immunol.* 14:43–64. https://doi.org/10.1038/cmi.2016.34

Boring, L., J. Gosling, S.W. Chensue, S.L. Kunkel, R.V. Farese Jr., H.E. Broxmeyer, and I.F. Charo. 1997. Impaired monocyte migration and reduced type 1 (Th1) cytokine responses in C-C chemokine receptor 2 knockout mice. *J. Clin. Invest.* 100:2552–2561. https://doi.org/10.1172/JCI119798

Borthwick, D.W., M. Shahbazian, Q.T. Krantz, J.R. Dorin, and S.H. Randell. 2001. Evidence for stem-cell niches in the tracheal epithelium. *Am. J. Respir. Cell Mol. Biol.* 24:662–670. https://doi.org/10.1165/ajrcmb.24.6.4217

Buchweitz, J.P., J.R. Harkema, and N.E. Kaminski. 2007. Time-dependent airway epithelial and inflammatory cell responses induced by influenza virus A/PR/8/34 in C57BL/6 mice. *Toxicol. Pathol.* 35:424–435. https://doi.org/10.1080/01926230701302558

Chera, S., L. Ghila, K. Dobretz, Y. Wenger, C. Bauer, W. Buzgariu, J.-C. Martinou, and B. Galliot. 2009. Apoptotic cells provide an unexpected source of Wnt3 signaling to drive hydra head regeneration. *Dev. Cell.* 17:279–289. https://doi.org/10.1016/j.devcel.2009.07.014

Cichoń, M.A., Z. Szentpetery, M.P. Caley, E.S. Papadakis, I.C. Mackenzie, C.H. Brennan, and E.A. O'Toole. 2014. The receptor tyrosine kinase Axl regulates cell-cell adhesion and stemness in cutaneous squamous cell carcinoma. *Oncogene.* 33:4185–4192. https://doi.org/10.1038/onc.2013.388

Crystal, R.G. 2014. Airway basal cells. The "smoking gun" of chronic obstructive pulmonary disease. *Am. J. Respir. Crit. Care Med.* 190:1355–1362. https://doi.org/10.1164/rccm.201408-1492PP

Demedts, I.K., T. Demoor, K.R. Bracke, G.F. Joos, and G.G. Brusselle. 2006. Role of apoptosis in the pathogenesis of COPD and pulmonary emphysema. *Respir. Res.* 7:53. https://doi.org/10.1186/1465-9921-7-53

Dye, J.A., and K.B. Adler. 1994. Effects of cigarette smoke on epithelial cells of the respiratory tract. *Thorax.* 49:825–834. https://doi.org/10.1136/thx.49.8.825

Evans, M.J., L.S. Van Winkle, M.V. Fanucchi, and C.G. Plopper. 2001. Cellular and molecular characteristics of basal cells in airway epithelium. *Exp. Lung Res.* 27:401–415. https://doi.org/10.1080/019021401300317125

Fan, Y., and A. Bergmann. 2008. Distinct mechanisms of apoptosis-induced compensatory proliferation in proliferating and differentiating tissues in the Drosophila eye. *Dev. Cell.* 14:399–410. https://doi.org/10.1016/j.devcel.2008.01.003

Fond, A.M., C.S. Lee, I.G. Schulman, R.S. Kiss, and K.S. Ravichandran. 2015. Apoptotic cells trigger a membrane-initiated pathway to increase ABCA1. *J. Clin. Invest.* 125:2748–2758. https://doi.org/10.1172/JCI80300

Fourgeaud, L., P.G. Través, Y. Tufail, H. Leal-Bailey, E.D. Lew, P.G. Burrola, P. Callaway, A. Zagórska, C.V. Rothlin, A. Nimmerjahn, and G. Lemke. 2016. TAM receptors regulate multiple features of microglial physiology. *Nature.* 532:240–244. https://doi.org/10.1038/nature17630

Fujimori, T., A.M. Grabiec, M. Kaur, T.J. Bell, N. Fujino, P.C. Cook, F.R. Svedberg, A.S. MacDonald, R.A. Maciewicz, D. Singh, and T. Hussell. 2015. The Axl receptor tyrosine kinase is a discriminator of macrophage function in the inflamed lung. *Mucosal Immunol.* 8:1021–1030. https://doi.org/10.1038/mi.2014.129

Fujino, N., H. Kubo, and R.A. Maciewicz. 2017. Phenotypic screening identifies Axl kinase as a negative regulator of an alveolar epithelial cell phenotype. *Lab. Invest.* 97:1047–1062. https://doi.org/10.1038/labinvest.2017.52

Gao, X., A.S. Bali, S.H. Randell, and B.L.M. Hogan. 2015. GRHL2 coordinates regeneration of a polarized mucociliary epithelium from basal stem cells. *J. Cell Biol.* 211:669–682. https://doi.org/10.1083/jcb.201506014

Gerdes, J., H. Lemke, H. Baisch, H.H. Wacker, U. Schwab, and H. Stein. 1984. Cell cycle analysis of a cell proliferation-associated human nuclear antigen defined by the monoclonal antibody Ki-67. *J. Immunol.* 133:1710–1715.

Grabiec, A.M., and T. Hussell. 2016. The role of airway macrophages in apoptotic cell clearance following acute and chronic lung inflammation. *Semin. Immunopathol.* 38:409–423. https://doi.org/10.1007/s00281-016-0555-3

Graham, D.K., D. DeRyckere, K.D. Davies, and H.S. Earp. 2014. The TAM family: phosphatidylserine sensing receptor tyrosine kinases gone awry in cancer. *Nat. Rev. Cancer.* 14:769–785. https://doi.org/10.1038/nrc3847

Hackett, N.R., R. Shaykhiev, M.S. Walters, R. Wang, R.K. Zwick, B. Ferris, B. Witover, J. Salit, and R.G. Crystal. 2011. The human airway epithelial basal cell transcriptome. *PLoS One.* 6:e18378. https://doi.org/10.1371/journal.pone.0018378

Hajj, R., T. Baranek, R. Le Naour, P. Lesimple, E. Puchelle, and C. Coraux. 2007. Basal cells of the human adult airway surface epithelium retain transit-amplifying cell properties. *Stem Cells.* 25:139–148. https://doi.org/10.1634/stemcells.2006-0288

Hochreiter-Hufford, A., and K.S. Ravichandran. 2013. Clearing the dead: apoptotic cell sensing, recognition, engulfment, and digestion. *Cold Spring Harb. Perspect. Biol.* 5:a008748. https://doi.org/10.1101/cshperspect.a008748

Hochreiter-Hufford, A.E., C.S. Lee, J.M. Kinchen, J.D. Sokolowski, S. Arandjelovic, J.A. Call, A.L. Klibanov, Z. Yan, J.W. Mandell, and K.S. Ravichandran. 2013. Phosphatidylserine receptor BAI1 and apoptotic cells as new promoters of myoblast fusion. *Nature.* 497:263–267. https://doi.org/10.1038/nature12135

Hodge, S., G. Hodge, M. Holmes, and P.N. Reynolds. 2005. Increased airway epithelial and T-cell apoptosis in COPD remains despite smoking cessation. *Eur. Respir. J.* 25:447–454. https://doi.org/10.1183/09031936.05.00077604

Hogg, J.C., P.T. Macklem, and W.M. Thurlbeck. 1968. Site and nature of airway obstruction in chronic obstructive lung disease. *N. Engl. J. Med.* 278:1355–1360. https://doi.org/10.1056/NEJM196806202782501

Hsu, H.-S., C.-C. Liu, J.-H. Lin, T.-W. Hsu, K. Su, and S.-C. Hung. 2014. Repair of naphthalene-induced acute tracheal injury by basal cells depends on β-catenin. *J. Thorac. Cardiovasc. Surg.* 148:322–332. https://doi.org/10.1016/j.jtcvs.2013.10.039

Ibricevic, A., A. Pekosz, M.J. Walter, C. Newby, J.T. Battaile, E.G. Brown, M.J. Holtzman, and S.L. Brody. 2006. Influenza virus receptor specificity and cell tropism in mouse and human airway epithelial cells. *J. Virol.* 80: 7469–7480. https://doi.org/10.1128/JVI.02677-05

Imai, K., B.A. Mercer, L.L. Schulman, J.R. Sonett, and J.M. D'Armiento. 2005. Correlation of lung surface area to apoptosis and proliferation in human emphysema. *Eur. Respir. J.* 25:250–258. https://doi.org/10.1183/09031936.05.00023704

Jan, Y.N., and L.Y. Jan. 1998. Asymmetric cell division. *Nature.* 392:775–778. https://doi.org/10.1038/33854

Jemielity, S., J.J. Wang, Y.K. Chan, A.A. Ahmed, W. Li, S. Monahan, X. Bu, M. Farzan, G.J. Freeman, D.T. Umetsu, et al. 2013. TIM-family proteins promote infection of multiple enveloped viruses through virion-associated phosphatidylserine. *PLoS Pathog.* 9:e1003232. https://doi.org/10.1371/journal.ppat.1003232

Kennedy, S.M., R.K. Elwood, B.J. Wiggs, P.D. Paré, and J.C. Hogg. 1984. Increased airway mucosal permeability of smokers. Relationship to airway reactivity. *Am. Rev. Respir. Dis.* 129:143–148. https://doi.org/10.1164/arrd.1984.129.1.143

Knight, D.A., and S.T. Holgate. 2003. The airway epithelium: structural and functional properties in health and disease. *Respirology.* 8:432–446. https://doi.org/10.1046/j.1440-1843.2003.00493.x

Lemke, G. 2013. Biology of the TAM receptors. *Cold Spring Harb. Perspect. Biol.* 5:a009076. https://doi.org/10.1101/cshperspect.a009076

Lemke, G., and C.V. Rothlin. 2008. Immunobiology of the TAM receptors. *Nat. Rev. Immunol.* 8:327–336. https://doi.org/10.1038/nri2303

Leopold, P.L., M.J. O'Mahony, X.J. Lian, A.E. Tilley, B.-G. Harvey, and R.G. Crystal. 2009. Smoking is associated with shortened airway cilia. *PLoS One.* 4:e8157. https://doi.org/10.1371/journal.pone.0008157

Lew, E.D., J. Oh, P.G. Burrola, I. Lax, A. Zagórska, P.G. Través, J. Schlessinger, and G. Lemke. 2014. Differential TAM receptor-ligand-phospholipid interactions delimit differential TAM bioactivities. *eLife.* 3:e03385. https://doi.org/10.7554/eLife.03385

Li, F., Q. Huang, J. Chen, Y. Peng, D.R. Roop, J.S. Bedford, and C.-Y. Li. 2010. Apoptotic cells activate the "phoenix rising" pathway to promote wound healing and tissue regeneration. *Sci. Signal.* 3:ra13. https://doi.org/10.1126/scisignal.2000634

Lu, Q., M. Gore, Q. Zhang, T. Camenisch, S. Boast, F. Casagranda, C. Lai, M.K. Skinner, R. Klein, G.K. Matsushima, et al. 1999. Tyro-3 family receptors are essential regulators of mammalian spermatogenesis. *Nature.* 398: 723–728. https://doi.org/10.1038/19554

Lumsden, A.B., A. McLean, and D. Lamb. 1984. Goblet and Clara cells of human distal airways: evidence for smoking induced changes in their numbers. *Thorax.* 39:844–849. https://doi.org/10.1136/thx.39.11.844

Makris, D., T. Vrekoussis, M. Izoldi, K. Alexandra, D. Katerina, T. Dimitris, A. Michalis, E. Tzortzaki, N.M. Siafakas, and N. Tzanakis. 2009. Increased apoptosis of neutrophils in induced sputum of COPD patients. *Respir. Med.* 103:1130–1135. https://doi.org/10.1016/j.rmed.2009.03.002

McCubbrey, A.L., and J.L. Curtis. 2013. Efferocytosis and lung disease. *Chest.* 143:1750–1757. https://doi.org/10.1378/chest.12-2413

Mercer, J., and A. Helenius. 2008. Vaccinia virus uses macropinocytosis and apoptotic mimicry to enter host cells. *Science.* 320:531–535. https://doi.org/10.1126/science.1155164

Morimoto, K., W.J. Janssen, and M. Terada. 2012. Defective efferocytosis by alveolar macrophages in IPF patients. *Respir. Med.* 106:1800–1803. https://doi.org/10.1016/j.rmed.2012.08.020

Pardo-Saganta, A., B.M. Law, P.R. Tata, J. Villoria, B. Saez, H. Mou, R. Zhao, and J. Rajagopal. 2015. Injury induces direct lineage segregation of functionally distinct airway basal stem/progenitor cell subpopulations. *Cell Stem Cell.* 16:184–197. https://doi.org/10.1016/j.stem.2015.01.002

Paul, M.K., B. Bisht, D.O. Darmawan, R. Chiou, V.L. Ha, W.D. Wallace, A.T. Chon, A.E. Hegab, T. Grogan, D.A. Elashoff, et al. 2014. Dynamic changes in intracellular ROS levels regulate airway basal stem cell homeostasis through Nrf2-dependent Notch signaling. *Cell Stem Cell.* 15:199–214. https://doi.org/10.1016/j.stem.2014.05.009

Peters, E.J., R. Morice, S.E. Benner, S. Lippman, J. Lukeman, J.S. Lee, J.Y. Ro, and W.K. Hong. 1993. Squamous metaplasia of the bronchial mucosa and its relationship to smoking. *Chest.* 103:1429–1432. https://doi.org/10.1378/chest.103.5.1429

Poon, I.K.H., C.D. Lucas, A.G. Rossi, and K.S. Ravichandran. 2014. Apoptotic cell clearance: basic biology and therapeutic potential. *Nat. Rev. Immunol.* 14:166–180. https://doi.org/10.1038/nri3607

Puchelle, E., J.-M. Zahm, J.-M. Tournier, and C. Coraux. 2006. Airway epithelial repair, regeneration, and remodeling after injury in chronic obstructive pulmonary disease. *Proc. Am. Thorac. Soc.* 3:726–733. https://doi.org/10.1513/pats.200605-126SF

Rawlins, E.L., T. Okubo, Y. Xue, D.M. Brass, R.L. Auten, H. Hasegawa, F. Wang, and B.L.M. Hogan. 2009. The role of Scgb1a1+ Clara cells in the long-term maintenance and repair of lung airway, but not alveolar, epithelium. *Cell Stem Cell.* 4:525–534. https://doi.org/10.1016/j.stem.2009.04.002

Rock, J.R., M.W. Onaitis, E.L. Rawlins, Y. Lu, C.P. Clark, Y. Xue, S.H. Randell, and B.L.M. Hogan. 2009. Basal cells as stem cells of the mouse trachea and human airway epithelium. *Proc. Natl. Acad. Sci. USA.* 106: 12771–12775. https://doi.org/10.1073/pnas.0906850106

Rock, J.R., S.H. Randell, and B.L.M. Hogan. 2010. Airway basal stem cells: a perspective on their roles in epithelial homeostasis and remodeling. *Dis. Model. Mech.* 3:545–556. https://doi.org/10.1242/dmm.006031

Rock, J.R., X. Gao, Y. Xue, S.H. Randell, Y.-Y. Kong, and B.L.M. Hogan. 2011. Notch-dependent differentiation of adult airway basal stem cells. *Cell Stem Cell.* 8:639–648. https://doi.org/10.1016/j.stem.2011.04.003

Ryan, D.M., T.L. Vincent, J. Salit, M.S. Walters, F. Agosto-Perez, R. Shaykhiev, Y. Strulovici-Barel, R.J. Downey, L.J. Buro-Auriemma, M.R. Staudt, et al. 2014. Smoking dysregulates the human airway basal cell transcriptome at COPD risk locus 19q13.2. *PLoS One.* 9:e88051. https://doi.org/10.1371/journal.pone.0088051

Ryoo, H.D., and A. Bergmann. 2012. The role of apoptosis-induced proliferation for regeneration and cancer. *Cold Spring Harb. Perspect. Biol.* 4: a008797. https://doi.org/10.1101/cshperspect.a008797

Schmidt, E.P., and R.M. Tuder. 2010. Role of Apoptosis in Amplifying Inflammatory Responses in Lung Diseases. *J. Cell Death.* 2010:41–53. https://doi.org/10.4137/JCD.S5375

Seong, S.-Y., and P. Matzinger. 2004. Hydrophobicity: an ancient damage-associated molecular pattern that initiates innate immune responses. *Nat. Rev. Immunol.* 4:469–478. https://doi.org/10.1038/nri1372

Shaykhiev, R., and R.G. Crystal. 2014a. Basal cell origins of smoking-induced airway epithelial disorders. *Cell Cycle.* 13:341–342. https://doi.org/10.4161/cc.27510

Shaykhiev, R., and R.G. Crystal. 2014b. Early events in the pathogenesis of chronic obstructive pulmonary disease. Smoking-induced reprogramming of airway epithelial basal progenitor cells. *Ann. Am. Thorac. Soc.* 11(Suppl 5):S252–S258. https://doi.org/10.1513/AnnalsATS.201402-049AW

Shaykhiev, R., F. Otaki, P. Bonsu, D.T. Dang, M. Teater, Y. Strulovici-Barel, J. Salit, B.-G. Harvey, and R.G. Crystal. 2011. Cigarette smoking reprograms apical junctional complex molecular architecture in the human airway epithelium in vivo. *Cell. Mol. Life Sci.* 68:877–892. https://doi.org/10.1007/s00018-010-0500-x

Shaykhiev, R., W.-L. Zuo, I. Chao, T. Fukui, B. Witover, A. Brekman, and R.G. Crystal. 2013. EGF shifts human airway basal cell fate toward a smoking-associated airway epithelial phenotype. *Proc. Natl. Acad. Sci. USA.* 110:12102–12107. https://doi.org/10.1073/pnas.1303058110

Soares, M.M., S.W. King, and P.E. Thorpe. 2008. Targeting inside-out phosphatidylserine as a therapeutic strategy for viral diseases. *Nat. Med.* 14:1357–1362. https://doi.org/10.1038/nm.1885

Staudt, M.R., L.J. Buro-Auriemma, M.S. Walters, J. Salit, T. Vincent, R. Shaykhiev, J.G. Mezey, A.E. Tilley, R.J. Kaner, M.W.Y. Ho, and R.G. Crystal. 2014. Airway Basal stem/progenitor cells have diminished capacity to regenerate airway epithelium in chronic obstructive pulmonary disease. *Am. J. Respir. Crit. Care Med.* 190:955–958. https://doi.org/10.1164/rccm.201406-1167LE

Tadokoro, T., Y. Wang, L.S. Barak, Y. Bai, S.H. Randell, and B.L.M. Hogan. 2014. IL-6/STAT3 promotes regeneration of airway ciliated cells from basal stem cells. *Proc. Natl. Acad. Sci. USA.* 111:E3641–E3649. https://doi.org/10.1073/pnas.1409781111

Tadokoro, T., X. Gao, C.C. Hong, D. Hotten, and B.L.M. Hogan. 2016. BMP signaling and cellular dynamics during regeneration of airway epithelium from basal progenitors. *Development.* 143:764–773. https://doi.org/10.1242/dev.126656

Tata, P.R., H. Mou, A. Pardo-Saganta, R. Zhao, M. Prabhu, B.M. Law, V. Vinarsky, J.L. Cho, S. Breton, A. Sahay, et al. 2013. Dedifferentiation of committed epithelial cells into stem cells in vivo. *Nature.* 503:218–223. https://doi.org/10.1038/nature12777

Tate, M.D., H.C. Schilter, A.G. Brooks, and P.C. Reading. 2011. Responses of mouse airway epithelial cells and alveolar macrophages to virulent and avirulent strains of influenza A virus. *Viral Immunol.* 24:77–88. https://doi.org/10.1089/vim.2010.0118

Van Brabandt, H., M. Cauberghs, E. Verbeken, P. Moerman, J.M. Lauweryns, and K.P. Van de Woestijne. 1983. Partitioning of pulmonary impedance

in excised human and canine lungs. *J. Appl. Physiol.* 55:1733–1742. https://doi.org/10.1152/jappl.1983.55.6.1733

Vandivier, R.W., T.R. Richens, S.A. Horstmann, A.M. deCathelineau, M. Ghosh, S.D. Reynolds, Y.-Q. Xiao, D.W. Riches, J. Plumb, E. Vachon, et al. 2009. Dysfunctional cystic fibrosis transmembrane conductance regulator inhibits phagocytosis of apoptotic cells with proinflammatory consequences. *Am. J. Physiol. Lung Cell. Mol. Physiol.* 297:L677–L686. https://doi.org/10.1152/ajplung.00030.2009

Vogelmeier, C.F., G.J. Criner, F.J. Martinez, A. Anzueto, P.J. Barnes, J. Bourbeau, B.R. Celli, R. Chen, M. Decramer, L.M. Fabbri, et al. 2017. Global Strategy for the Diagnosis, Management, and Prevention of Chronic Obstructive Lung Disease 2017 Report. GOLD Executive Summary. *Am. J. Respir. Crit. Care Med.* 195:557–582. https://doi.org/10.1164/rccm.201701-0218PP

Voynow, J.A., B.M. Fischer, B.C. Roberts, and A.D. Proia. 2005. Basal-like cells constitute the proliferating cell population in cystic fibrosis airways. *Am. J. Respir. Crit. Care Med.* 172:1013–1018. https://doi.org/10.1164/rccm.200410-1398OC

Watson, J.K., S. Rulands, A.C. Wilkinson, A. Wuidart, M. Ousset, A. Van Keymeulen, B. Göttgens, C. Blanpain, B.D. Simons, and E.L. Rawlins. 2015. Clonal Dynamics Reveal Two Distinct Populations of Basal Cells in Slow-Turnover Airway Epithelium. *Cell Reports.* 12:90–101. https://doi.org/10.1016/j.celrep.2015.06.011

Williams, S.E., S. Beronja, H.A. Pasolli, and E. Fuchs. 2011. Asymmetric cell divisions promote Notch-dependent epidermal differentiation. *Nature.* 470:353–358. https://doi.org/10.1038/nature09793

Yanai, M., K. Sekizawa, T. Ohrui, H. Sasaki, and T. Takishima. 1992. Site of airway obstruction in pulmonary disease: direct measurement of intrabronchial pressure. *J. Appl. Physiol.* 72:1016–1023. https://doi.org/10.1152/jappl.1992.72.3.1016

You, Y., E.J. Richer, T. Huang, and S.L. Brody. 2002. Growth and differentiation of mouse tracheal epithelial cells: selection of a proliferative population. *Am. J. Physiol. Lung Cell. Mol. Physiol.* 283:L1315–L1321. https://doi.org/10.1152/ajplung.00169.2002

Zagórska, A., P.G. Través, E.D. Lew, I. Dransfield, and G. Lemke. 2014. Diversification of TAM receptor tyrosine kinase function. *Nat. Immunol.* 15:920–928. https://doi.org/10.1038/ni.2986

Zhang, Z., J.C. Lee, L. Lin, V. Olivas, V. Au, T. LaFramboise, M. Abdel-Rahman, X. Wang, A.D. Levine, J.K. Rho, et al. 2012. Activation of the AXL kinase causes resistance to EGFR-targeted therapy in lung cancer. *Nat. Genet.* 44:852–860. https://doi.org/10.1038/ng.2330

Zhao, R., T.R. Fallon, S.V. Saladi, A. Pardo-Saganta, J. Villoria, H. Mou, V. Vinarsky, M. Gonzalez-Celeiro, N. Nunna, L.P. Hariri, et al. 2014. Yap tunes airway epithelial size and architecture by regulating the identity, maintenance, and self-renewal of stem cells. *Dev. Cell.* 30:151–165. https://doi.org/10.1016/j.devcel.2014.06.004